

Energy relaxation approximation for the compressible multicomponent flows in thermal nonequilibrium

Claude Marmignon · Fabio Naddei · Florent Renac

Received: date / Accepted: date

Abstract This work concerns the numerical approximation with a finite volume method of inviscid, nonequilibrium, high-temperature flows in multiple space dimensions. It is devoted to the analysis of the numerical scheme for the approximation of the hyperbolic system in homogeneous form. We derive a general framework for the design of numerical schemes for this model from numerical schemes for the monocomponent compressible Euler equations for a polytropic gas. Under a very simple condition on the adiabatic exponent of the polytropic gas, the scheme for the multicomponent system enjoys the same properties as the one for the monocomponent system: discrete entropy inequality, positivity of the partial densities and internal energies, discrete maximum principle on the mass fractions, and discrete minimum principle on the entropy. Our approach extends the relaxation of energy [Coquel and Perthame, *SIAM J. Numer. Anal.*, 35 (1998), 2223–2249] to the multicomponent Euler system. In the limit of instantaneous relaxation we show that the solution formally converges to a unique and stable equilibrium solution to the multicomponent Euler equations. We then use this framework to design numerical schemes from three schemes for the polytropic Euler system: the Godunov exact Riemann solver [Godunov, *Math. Sbornik*, 47 (1959), 271–306] and the HLL [Harten et al., *SIAM Rev.*, 25 (1983), 35–61] and pressure relaxation based [Bouchut, *Nonlinear stability of finite volume methods for hyperbolic conservation laws and well-balanced schemes for sources*, *Frontiers in Mathematics*, Birkhäuser, 2004] approximate Riemann solvers. Numerical experiments in one and two space dimensions on flows with discontinuous solutions support the conclusions of our analysis and highlight stability, robustness and convergence of the scheme.

Keywords Compressible multicomponent flows · thermal nonequilibrium · relaxation of hyperbolic systems · finite volume method · relaxation scheme

C. Marmignon
DAAA, ONERA, Université Paris Saclay, F-92322 Châtillon, France

F. Naddei
DAAA, ONERA, Université Paris Saclay, F-92322 Châtillon, France

F. Renac
DAAA, ONERA, Université Paris Saclay, F-92322 Châtillon, France
E-mail: florent.renac@onera.fr

Mathematics Subject Classification (2000) 65M12 · 65M70 · 76T10

1 Introduction

We are here interested in finite volume methods to simulate inviscid hypersonic high-temperature flows. Such simulations are of strong significance in many applications (e.g., hypersonic air vehicles [32], reentry vehicles [2], meteoroid entry into atmosphere [29]) and scientific topics (e.g., weakly ionized gases, heat transfer [39], boundary layer stability [33], shock propagation [30]) related to hypersonic flows. For such flows, effects of thermal and chemical nonequilibrium are important and cannot be modeled by the monocomponent compressible Euler equations for a polytropic gas. Real gas models usually include multiple temperatures, chemical reaction rates and vibrational relaxation effects [20,2]. We here focus on issues related to the numerical treatment of the convective fluxes due to their hyperbolic nature and on the capture of associated features such as strong shocks. We therefore consider thermal nonequilibrium only and neglect chemical nonequilibrium and relaxation of vibration energies that are associated to numerical issues of different nature.

The numerical analysis of hypersonic flows is usually challenging because the characteristic time scales of the chemical reactions and molecular vibrations may be quite different from the characteristic time scale of the flow field. Taking into account the variations in the chemical composition and internal energy modes of a fluid requires to resolve the mass fractions and vibration energies. The thermodynamic properties then depend on these variables which complicates the design of numerical schemes with sought-after properties such as robustness (i.e., that keeps positivity of partial densities and internal and vibration energies), stability from a discrete entropy inequality, maximum principle on the mass fractions, etc.

The design of numerical schemes for the approximation of the compressible multicomponent Euler equations has been an active field of research over the past decades. Park proposed an implicit time marching associated to central differencing of ionized flows [36], while finite volume discretizations have been widely developed with flux splitting techniques [7,4,34,45], Jacobian based methods such as the Roe method [10,21], the AUSM scheme [19], relaxation based approximate Riemann solvers (ARS) [43], etc. High-order extensions have been proposed with the second-order MUSCL method [15], ENO and WENO reconstructions [50,14], interface capturing schemes [1,31]. Shock fitting techniques have also been addressed in [39]. In this work we will consider the design of finite volume schemes based on ARS.

To ensure entropy stability and robustness when using ARS such as the HLL [27], Roe [42], Rusanov [44], relaxation [3,9] schemes, etc., one needs an estimation from above of the maximum wave speeds in the Riemann problem. However, fast estimates such as the two-rarefaction approximation [51, Ch. 9], the iterative algorithm from [25], or the one based on eigenvalues of the Roe linearisation [16] will require time-consuming Newton-Raphson iterations when the equation of state (EOS) differs in the left and right states due to different species compositions. In [13] a relaxation technique is applied to the multicomponent Euler system which allows the use of monocomponent schemes for each component and associated EOS and the scheme inherits properties from the monocomponent scheme.

However, this technique requires to compute as many monocomponent schemes as there are species which can become time consuming. Moreover, the entropy of the relaxation system is proved to be convex for constant mass fractions only which is valid for isolated shocks, but fails for interactions of shocks with material interfaces. Here we consider the energy relaxation technique introduced in [11] for the approximation of the monocomponent compressible Euler equations with a general EOS. In this method, one considers a decomposition of the internal energy including the energy for a polytropic gas thus relaxing the general EOS. The method then allows the design of numerical schemes by using classical numerical fluxes for polytropic gases coupled to instantaneous relaxation of the energy.

In this work, we extend this method to our model and show how to define a numerical scheme from a scheme for the polytropic gas dynamics through a simple formula (equation (4.25)) which corresponds to a splitting of hyperbolic and relaxation operators. In the limit of instantaneous relaxation we show that the solution of the energy relaxation approximation formally converges to a unique and stable equilibrium solution to the multicomponent Euler equations which justify the splitting. By defining the adiabatic exponent of the polytropic gas as an upper bound of the possible values of adiabatic exponent of the mixture, the scheme for the multicomponent system inherits the properties of the scheme for the monocomponent system: discrete entropy inequality, positivity of the partial densities and internal energies, discrete maximum principle on the mass fractions, and discrete minimum principle on the entropy. An attempt to apply the energy relaxation approximation to the multicomponent Euler system for a fluid mixture in thermal equilibrium has been made in [40]. However, this work did not provide a general framework to build numerical schemes. The closure laws for the fluid mixture indeed prevent the derivation of a strictly convex entropy for the relaxation system which in turn prevents to apply stability theorems [5] to the relaxation process. As a consequence the well-posedness of the instantaneous relaxation process has not been investigated either. On the other hand, the present work successfully addresses this property and may use any polytropic three-point scheme.

The paper is organized as follows. Section 2 presents the multicomponent compressible Euler system in thermal nonequilibrium and the entropy pair. The unstructured finite volume scheme and the three-point scheme are described in section 3. We introduce and analyze the relaxation in energy approximation in section 4 that we use in section 5 to derive three numerical fluxes for the finite volume scheme. These three schemes are then assessed by numerical experiments in one and two space dimensions in section 6 and concluding remarks about this work are given in section 7.

2 Model problem

2.1 Governing equations and thermodynamic model

Let $\Omega \subset \mathbb{R}^d$ be a bounded domain in d space dimensions, we consider the multi-species and multi-temperature model for flows in thermal nonequilibrium [37]. Let the IBVP described by the multicomponent compressible Euler system for a

mixture of n_s species

$$\partial_t \mathbf{u} + \nabla \cdot \mathbf{f}(\mathbf{u}) = 0, \quad \text{in } \Omega \times (0, \infty), \quad (2.1a)$$

$$\mathbf{u}(\cdot, 0) = \mathbf{u}_0(\cdot), \quad \text{in } \Omega, \quad (2.1b)$$

with some boundary conditions to be prescribed on $\partial\Omega$ (see section 5.4). Here

$$\mathbf{u} = \begin{pmatrix} \boldsymbol{\rho} \\ \rho \mathbf{v} \\ \rho E \\ \rho \mathbf{e}_v \end{pmatrix}, \quad \mathbf{f}(\mathbf{u}) = \begin{pmatrix} \rho \mathbf{v}^\top \\ \rho \mathbf{v} \mathbf{v}^\top + p \mathbf{I} \\ (\rho E + p) \mathbf{v}^\top \\ \rho \mathbf{e}_v \mathbf{v}^\top \end{pmatrix}, \quad (2.2)$$

denote the conserved variables and the convective fluxes with $\boldsymbol{\rho} = (\rho_1, \dots, \rho_{n_s})^\top$ the vector of densities of the n_s species, while ρ , \mathbf{v} in \mathbb{R}^d , and E denote the density, velocity vector, and total specific energy of the mixture, respectively. By $\rho \mathbf{e}_v = (\rho_1 e_1^v, \dots, \rho_{n_d} e_{n_d}^v)^\top$ we denote the vector of partial vibration energies of the n_d diatomic species that are in thermal nonequilibrium. Each partial vibration energy is linked to the associated vibration temperature T_β^v through

$$e_\beta^v(T_\beta^v) = r_\beta \frac{\vartheta_\beta^v}{\exp\left(\frac{\vartheta_\beta^v}{T_\beta^v}\right) - 1}, \quad r_\beta = \frac{\mathcal{R}}{M_\beta}, \quad (2.3)$$

where ϑ_β^v is the characteristic harmonic oscillator temperature, and r_β is the gas constant of the species β with \mathcal{R} is the universal gas constant and M_β the molecular weight of the species.

The mixture density, pressure and vibration energy are defined from quantities of the individual species through

$$\rho = \sum_{\alpha=1}^{n_s} \rho_\alpha = \rho \sum_{\alpha=1}^{n_s} Y_\alpha, \quad p = \sum_{\alpha=1}^{n_s} p_\alpha, \quad \rho e_v = \sum_{\beta=1}^{n_d} \rho_\beta e_\beta^v, \quad (2.4)$$

where $Y_\alpha = \frac{\rho_\alpha}{\rho}$ denotes the mass fraction of the α th species, so we have

$$\sum_{\alpha=1}^{n_s} Y_\alpha = 1. \quad (2.5)$$

The specific total energy of the mixture reads

$$E = h_0 + e_t + e_v + e_c, \quad h_0 = \sum_{\alpha=1}^{n_s} Y_\alpha h_\alpha^0, \quad e_t = \sum_{\alpha=1}^{n_s} Y_\alpha e_\alpha^t, \quad e_c = \frac{1}{2} \mathbf{v} \cdot \mathbf{v}, \quad (2.6)$$

where $h_\alpha^0 \geq 0$ is the enthalpy of formation of species α , $e_\alpha^t = C_{v_\alpha}^t T$ denotes the internal translation-rotation energy with $C_{v_\alpha}^t = \frac{3}{2} r_\alpha$ for a monoatomic species and $C_{v_\alpha}^t = \frac{5}{2} r_\alpha$ for diatomic molecules. The EOS for the mixture pressure in (2.4) is given by the Dalton's law and the partial pressures are assumed to obey polytropic ideal gas EOSs:

$$p = \sum_{\alpha=1}^{n_s} \rho_\alpha r_\alpha T = \rho r(\mathbf{Y}) T, \quad r(\mathbf{Y}) = \mathcal{Z}(\mathbf{Y}) \mathcal{R}, \quad \mathcal{Z}(\mathbf{Y}) = \sum_{\alpha=1}^{n_s} \frac{Y_\alpha}{M_\alpha}, \quad (2.7)$$

where $\mathbf{Y} = (Y_1, \dots, Y_{n_s})^\top$. Note that the pressure may be also written as

$$p(\mathbf{Y}, \rho, e_t) = (\gamma(\mathbf{Y}) - 1)\rho e_t, \quad (2.8)$$

with

$$\gamma(\mathbf{Y}) = \frac{r(\mathbf{Y})}{C_{v_t}(\mathbf{Y})} + 1, \quad r(\mathbf{Y}) \stackrel{(2.7)}{=} \sum_{\alpha=1}^{n_s} Y_\alpha r_\alpha, \quad C_{v_t}(\mathbf{Y}) = \sum_{\alpha=1}^{n_s} Y_\alpha C_{v_\alpha}^t. \quad (2.9)$$

This induces the following bounds on $\gamma(\mathbf{Y})$:

$$\frac{7}{5} \leq \gamma(\mathbf{Y}) \leq \frac{5}{3} \quad \forall 0 \leq Y_{1 \leq \alpha \leq n_s} \leq 1. \quad (2.10)$$

System (2.1a) is hyperbolic in the direction \mathbf{n} in \mathbb{R}^d over the set of states [34]

$$\Omega^a = \{\mathbf{u} \in \mathbb{R}^{n_s+n_d+d+1} : \rho_{1 \leq \alpha \leq n_s} > 0, \mathbf{v} \in \mathbb{R}^d, e_t > 0, e_{1 \leq \beta \leq n_d}^v > 0\}, \quad (2.11)$$

with eigenvalues $\lambda_1 = \mathbf{v} \cdot \mathbf{n} - c \leq \lambda_2 = \dots = \lambda_{n_s+n_d+d} = \mathbf{v} \cdot \mathbf{n} \leq \lambda_{n_s+n_d+d+1} = \mathbf{v} \cdot \mathbf{n} + c$, where λ_1 and $\lambda_{n_s+n_d+d+1}$ are associated to genuinely nonlinear fields and $\lambda_{2 \leq i \leq n_s+n_d+d}$ to linearly degenerate fields. The frozen sound speed reads

$$c(\mathbf{Y}, e_t) = \sqrt{\gamma(\mathbf{Y})(\gamma(\mathbf{Y}) - 1)} e_t. \quad (2.12)$$

Finally note that we are assuming in (2.11) that the partial densities are positive which would prevent vanishing phases: $\rho_\alpha = 0$ for some α . When such situation occurs the partial velocities, pressure and energies of the species also vanish and this is equivalent to removing the species in the model (2.1) so $\rho_\alpha > 0$ in (2.11) is justified and do not exclude vanishing phases.

2.2 Entropy pair

Solutions to (2.1) should satisfy an entropy inequality

$$\partial_t \eta(\mathbf{u}) + \nabla \cdot \mathbf{q}(\mathbf{u}) \leq 0 \quad (2.13)$$

for some entropy – entropy flux pair (η, \mathbf{q}) with $\eta(\cdot)$ a strictly convex function and $\boldsymbol{\eta}'(\mathbf{u})^\top \mathbf{f}'_i(\mathbf{u}) = \mathbf{q}'_i(\mathbf{u})^\top$ for $1 \leq i \leq d$. In this section we recall the entropy pair for (2.1) derived in [18] and then prove convexity of the entropy.

Following [18], the entropy for a mixture with internal degrees of freedom in nonequilibrium is the sum of associated entropies defined by their differential forms

$$\mathbb{T} ds_\alpha^t = de_\alpha^t + p_\alpha d\tau_\alpha \quad \forall 1 \leq \alpha \leq n_s, \quad (2.14a)$$

$$\mathbb{T}_\beta^v ds_\beta^v = de_\beta^v \quad \forall 1 \leq \beta \leq n_d, \quad (2.14b)$$

with $\tau_\alpha = \frac{1}{\rho_\alpha}$ the covolume of the species α . The entropy pair in (2.13) reads

$$\eta(\mathbf{u}) = -\rho s(\mathbf{u}), \quad \mathbf{q}(\mathbf{u}) = -\rho s(\mathbf{u}) \mathbf{v}, \quad s \equiv \sum_{\alpha=1}^{n_s} Y_\alpha s_\alpha^t + \sum_{\beta=1}^{n_d} Y_\beta s_\beta^v. \quad (2.15)$$

Let $g_\alpha^t = e_\alpha^t + p_\alpha \tau_\alpha - T s_\alpha^t$ be the free Gibbs energy of the α th species and $g_\beta^v = e_\beta^v - T s_\beta^v$, using the differential forms (2.14) we obtain

$$\begin{aligned} T \sum_{\alpha=1}^{n_s} d(\rho_\alpha s_\alpha^t) &= \sum_{\alpha=1}^{n_s} d(\rho_\alpha e_\alpha^t) - (e_\alpha^t + p_\alpha \tau_\alpha - T s_\alpha^t) d\rho_\alpha \\ &= d(\rho E) - d(\rho e_v) - \mathbf{v} \cdot d(\rho \mathbf{v}) - \sum_{\alpha=1}^{n_s} (g_\alpha^t + h_\alpha^0 - e_c) d\rho_\alpha, \\ \sum_{\beta=1}^{n_d} d(\rho_\beta s_\beta^v) &= \sum_{\beta=1}^{n_d} (s_\beta^v(e_\beta^v) - e_\beta^v \theta_\beta^v) d\rho_\beta + \theta_\beta^v d(\rho_\beta e_\beta^v), \end{aligned}$$

with $\theta_\beta^v = \frac{1}{T_\beta^v} = s_\beta^{v'}(e_\beta^v)$, so the entropy variables read

$$\boldsymbol{\eta}'(\mathbf{u}) := \left(\frac{\boldsymbol{\eta}(\mathbf{u})}{\partial \mathbf{u}} \right)^\top = \begin{pmatrix} C_{v_1}^t + r_1 - s_1^t + \psi_1 \theta_1^v g_1^v + (h_1^0 - e_c) \theta \\ \vdots \\ C_{v_{n_s}}^t + r_{n_s} - s_{n_s}^t + \psi_{n_s} \theta_{n_s}^v g_{n_s}^v + (h_{n_s}^0 - e_c) \theta \\ \theta \mathbf{v} \\ -\theta \\ \theta - \theta_1^v \\ \vdots \\ \theta - \theta_{n_d}^v \end{pmatrix}, \quad (2.18)$$

and we obtain for $\frac{\partial \boldsymbol{\eta}'(\mathbf{u})}{\partial \mathbf{z}}$

$$\begin{pmatrix} \frac{r_1}{\rho_1} & & 0 & -\theta \mathbf{v}^\top & -C_{v_1}^t \theta - (h_1^0 - e_c) \theta^2 & e_1^v s_1^{v''}(e_1^v) & & 0 \\ & \ddots & & \vdots & \vdots & \vdots & \ddots & \\ & & \frac{r_{n_d}}{\rho_{n_d}} & -\theta \mathbf{v}^\top & -C_{v_{n_d}}^t \theta - (h_{n_d}^0 - e_c) \theta^2 & 0 & & e_{n_d}^v s_{n_d}^{v''}(e_{n_d}^v) \\ & & & \vdots & \vdots & \vdots & \ddots & \\ 0 & & & \frac{r_{n_s}}{\rho_{n_s}} & -\theta \mathbf{v}^\top & -C_{v_{n_s}}^t \theta - (h_{n_s}^0 - e_c) \theta^2 & 0 & \cdots & 0 \\ 0 & \cdots & \cdots & 0 & \theta \mathbf{I}_d & -\theta^2 \mathbf{v} & 0 & \cdots & 0 \\ 0 & \cdots & \cdots & 0 & 0 & \theta^2 & 0 & \cdots & 0 \\ 0 & \cdots & 0 & \cdots & 0 & -\theta^2 & -s_1^{v''}(e_1^v) & & 0 \\ \vdots & \ddots & \vdots & \ddots & \vdots & \vdots & \ddots & & \\ 0 & \cdots & 0 & \cdots & 0 & -\theta^2 & 0 & & -s_{n_d}^{v''}(e_{n_d}^v) \end{pmatrix},$$

so it may be easily checked that (2.17) holds true. \square

Finally, let $\tau = \frac{1}{\rho}$ be the covolume of the mixture. Using $\frac{e_\alpha^t}{C_{v_\alpha}^t} = \frac{e_t}{C_{v_t}(\mathbf{Y})} = T$ and $Y_\alpha \tau_\alpha = \tau$, for all α , in (2.16) the entropy of the mixture in (2.15) may be

written as

$$\begin{aligned} s(\mathbf{Y}, \tau, e_t, \mathbf{e}_v) &= \sum_{\alpha=1}^{n_s} Y_\alpha C_{v_\alpha}^t \ln \left(\frac{C_{v_\alpha}^t}{C_{v_t}(\mathbf{Y})} e_t \right) + Y_\alpha r_\alpha \ln \left(\frac{\tau}{Y_\alpha} \right) + s_v(\mathbf{Y}, \mathbf{e}_v) \\ &= C_{v_t}(\mathbf{Y}) \ln e_t + r(\mathbf{Y}) \ln \tau + K(\mathbf{Y}) + s_v(\mathbf{Y}, \mathbf{e}_v), \end{aligned} \quad (2.19a)$$

$$K(\mathbf{Y}) = \sum_{\alpha=1}^{n_s} Y_\alpha \left(C_{v_\alpha}^t \ln \left(\frac{C_{v_\alpha}^t}{C_{v_t}(\mathbf{Y})} \right) - r_\alpha \ln Y_\alpha \right), \quad (2.19b)$$

$$s_v(\mathbf{Y}, \mathbf{e}_v) = \sum_{\beta=1}^{n_d} Y_\beta s_\beta^v(e_\beta^v). \quad (2.19c)$$

3 Finite volume method

We consider finite volume schemes for unstructured meshes $\Omega_h \subset \mathbb{R}^d$ of the form

$$\mathbf{U}_\kappa^{n+1} - \mathbf{U}_\kappa^n + \frac{\Delta t^{(n)}}{|\kappa|} \sum_{e \in \partial \kappa} |e| \mathbf{h}(\mathbf{U}_\kappa^n, \mathbf{U}_{\kappa_e^+}^n, \mathbf{n}_e) = 0 \quad \forall \kappa \in \Omega_h, n \geq 0, \quad (3.1)$$

for the discretization of (2.1a). Here \mathbf{U}_κ^{n+1} approximates the averaged solution in the cell κ at time $t^{(n+1)} = t^{(n)} + \Delta t^{(n)}$, $\Delta t^{(n)} > 0$ is the time step, \mathbf{n}_e is the unit outward normal vector on the edge e in $\partial \kappa$, and κ_e^+ the neighboring cell sharing the interface e (see fig. 3.1). We assume that each element is shape-regular in the sense of [6]: the ratio of the radius of the largest inscribed ball to the diameter is bounded by below by a positive constant independent of the mesh. The initial condition for (3.1) reads

$$\mathbf{U}_\kappa^0 = \frac{1}{|\kappa|} \int_\kappa \mathbf{u}_0(\mathbf{x}) dV \quad \forall \kappa \in \Omega_h.$$

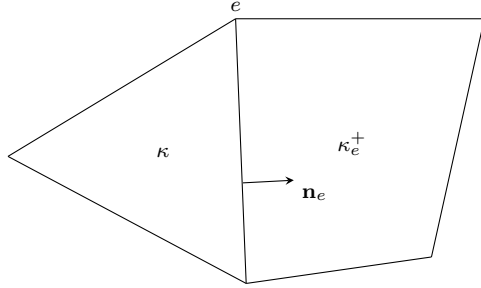


Fig. 3.1: Notations for the mesh for $d = 2$.

It is convenient to also consider three-point numerical schemes of the form

$$\mathbf{U}_j^{n+1} - \mathbf{U}_j^n + \frac{\Delta t^{(n)}}{\Delta x} (\mathbf{h}(\mathbf{U}_j^n, \mathbf{U}_{j+1}^n, \mathbf{n}) - \mathbf{h}(\mathbf{U}_{j-1}^n, \mathbf{U}_j^n, \mathbf{n})) = 0, \quad (3.2)$$

where \mathbf{U}_j^n approximates the averaged solution in the j th cell at time $t^{(n)}$, Δx is the space step. In particular we are looking for schemes (3.2) that have the following properties under a given condition on the time step

$$\frac{\Delta t^{(n)}}{\Delta x} \max_{j \in \mathbb{Z}} |\lambda(\mathbf{U}_j^n)| \leq \frac{1}{2}, \quad (3.3)$$

where $|\lambda(\cdot)|$ corresponds to the maximum absolute value of the wave speeds (and will be defined in section 5): the scheme is

- (i) *consistent* with (2.1a) and *conservative* which requires the numerical flux to be consistent:

$$\mathbf{h}(\mathbf{u}, \mathbf{u}, \mathbf{n}) = \mathbf{f}(\mathbf{u}) \cdot \mathbf{n} \quad \forall \mathbf{u} \in \Omega^a, \quad (3.4)$$

and conservative:

$$\mathbf{h}(\mathbf{u}^-, \mathbf{u}^+, \mathbf{n}) = -\mathbf{h}(\mathbf{u}^+, \mathbf{u}^-, -\mathbf{n}) \quad \forall \mathbf{u}^\pm \in \Omega^a; \quad (3.5)$$

- (ii) *Lipschitz continuous* which also requires the numerical flux to be Lipschitz continuous;
- (iii) *entropy stable (ES)* for the pair (η, \mathbf{q}) in (2.13): it satisfies the inequality

$$\eta(\mathbf{U}_j^{n+1}) - \eta(\mathbf{U}_j^n) + \frac{\Delta t^{(n)}}{\Delta x} (Q(\mathbf{U}_j^n, \mathbf{U}_{j+1}^n, \mathbf{n}) - Q(\mathbf{U}_{j-1}^n, \mathbf{U}_j^n, \mathbf{n})) \leq 0, \quad (3.6)$$

with some conservative and consistent entropy numerical flux $Q(\mathbf{u}, \mathbf{u}, \mathbf{n}) = \mathbf{q}(\mathbf{u}) \cdot \mathbf{n}$;

- (iv) *robust*: the solution remains in the set of states (2.11): $\mathbf{U}_{j \in \mathbb{Z}}^n$ in Ω^a implies $\mathbf{U}_{j \in \mathbb{Z}}^{n+1}$ in Ω^a ;
- (v) and it satisfies a *discrete maximum principle on the mass fractions*:

$$\min(Y_{\alpha_{j-1}}^n, Y_{\alpha_j}^n, Y_{\alpha_{j+1}}^n) \leq Y_{\alpha_j}^{n+1} \leq \max(Y_{\alpha_{j-1}}^n, Y_{\alpha_j}^n, Y_{\alpha_{j+1}}^n) \quad \forall 1 \leq \alpha \leq n_s, \quad (3.7)$$

- (vi) together with a *minimum principle on the specific entropy* in (2.15) [47, 24]:

$$s(\mathbf{U}_j^{n+1}) \geq \min(s(\mathbf{U}_{j-1}^n), s(\mathbf{U}_j^n), s(\mathbf{U}_{j+1}^n)). \quad (3.8)$$

Then it is a classical matter (see e.g. [38, 48, 49, 22] and references therein) that the finite volume scheme (3.1) with the same numerical flux enjoys similar properties. Under the following condition on the time step

$$\Delta t^{(n)} \max_{\kappa \in \Omega_h} \frac{|\partial \kappa|}{|\kappa|} \max_{e \in \partial \kappa} |\lambda(\mathbf{U}_{\kappa^\pm}^n)| \leq \frac{1}{2}, \quad |\partial \kappa| := \sum_{e \in \partial \kappa} |e|, \quad (3.9)$$

the scheme is robust and is a convex combination of updates of three-point schemes (3.2):

$$\mathbf{U}_\kappa^{n+1} = \sum_{e \in \partial \kappa} \frac{|e|}{|\partial \kappa|} \left(\mathbf{U}_\kappa^n - \frac{\Delta t^{(n)} |\partial \kappa|}{|\kappa|} (\mathbf{h}(\mathbf{U}_\kappa^n, \mathbf{U}_{\kappa_e^+}^n, \mathbf{n}_e) - \mathbf{h}(\mathbf{U}_\kappa^n, \mathbf{U}_\kappa^n, \mathbf{n}_e)) \right), \quad (3.10)$$

with weights $\frac{|e|}{|\partial \kappa|}$. Therefore, the scheme (3.1) also satisfies the discrete minimum and maximum principles together with the entropy inequality

$$\eta(\mathbf{U}_\kappa^{n+1}) - \eta(\mathbf{U}_\kappa^n) + \frac{\Delta t^{(n)}}{|\kappa|} \sum_{e \in \partial \kappa} |e| Q(\mathbf{U}_\kappa^n, \mathbf{U}_{\kappa_e^+}^n, \mathbf{n}_e) \leq 0, \quad (3.11)$$

consistent with (2.13).

In the following we design finite volume schemes (3.1) with the CFL condition (3.9) by first designing three-point schemes (3.2) that satisfy properties (i) to (vi) with (3.3).

4 Energy relaxation approximation

In this section we derive a general framework that allows the use of standard numerical schemes for the classical gas dynamics with a polytropic ideal gas EOS. The main results are summarized in theorem 4.3 and show how to build a three-point scheme for (2.1a) that enjoys the properties (i) to (vi) in section 3 from a three-point scheme for the compressible Euler equations with a polytropic law.

We here extend the energy relaxation approximation for the multicomponent Euler system [11] to include the vibration energies (section 4.1) and introduce a convex entropy in section 4.2. Section 4.3 is devoted to the analysis of solutions to the relaxation system close to equilibrium. In the limit of instantaneous relaxation, we prove that:

- solutions to the relaxation system formally converge to a unique and stable equilibrium solution to the multicomponent Euler equations (2.1a) (theorem 4.1);
- this equilibrium corresponds to a global minimum of the relaxation entropy which satisfies a variational principle (lemma 4.3);
- small perturbations close to the equilibrium are associated to dissipative processes in (2.1a) (theorem 4.2).

These results are then used to infer a numerical scheme for (2.1a) from one for the relaxation system (section 4.4) based on a splitting of the hyperbolic and relaxation operators.

4.1 Energy relaxation system

Following the energy relaxation method introduced in [11], we consider the system

$$\partial_t \mathbf{w}^\epsilon + \nabla \cdot \mathbf{g}(\mathbf{w}^\epsilon) = -\frac{1}{\epsilon} (\mathbf{w}^\epsilon - \mathcal{M}(\mathbf{w}^\epsilon)), \quad (4.1)$$

and we will denote by (4.1) $_{\epsilon \rightarrow \infty}$ the system in homogeneous form, i.e., with $\epsilon \rightarrow \infty$. Here

$$\mathbf{w} = \begin{pmatrix} \rho \\ \rho \mathbf{v} \\ \rho E_r \\ \rho \mathbf{e}_v \\ \rho e_s \end{pmatrix}, \quad \mathbf{g}(\mathbf{w}) = \begin{pmatrix} \rho \mathbf{v}^\top \\ \rho \mathbf{v} \mathbf{v}^\top + p_r(\rho, e_r) \mathbf{I} \\ (\rho E_r + p_r(\rho, e_r)) \mathbf{v}^\top \\ \rho \mathbf{e}_v \mathbf{v}^\top \\ \rho e_s \mathbf{v}^\top \end{pmatrix}, \quad \mathbf{w} - \mathcal{M}(\mathbf{w}) = \begin{pmatrix} 0 \\ 0 \\ \rho(F(\mathbf{Y}, e_r) - e_s) \\ 0 \\ \rho(e_s - F(\mathbf{Y}, e_r)) \end{pmatrix},$$

with $\epsilon > 0$ the relaxation time scale, and

$$p_r(\rho, e_r) = (\gamma - 1)\rho e_r, \quad e_r = E_r - e_c. \quad (4.2)$$

Solutions to (4.1) satisfy the additional conservation law

$$\partial_t \rho^\epsilon + \nabla \cdot (\rho^\epsilon \mathbf{v}^\epsilon) = 0, \quad (4.3)$$

for the mixture density so the variables ρ , $\rho \mathbf{v}$ and ρE_r are uncoupled from \mathbf{Y} and \mathbf{e}_v and coupled to e_s through the relaxation source terms only. This is an important aspect of the model (4.1) and also allows to interpret E_r , e_r , and p_r as the energies and pressure of a polytropic EOS.

From (2.10) we set γ as

$$\gamma > \max_{0 \leq Y_1 \leq \alpha \leq n_s \leq 1} \gamma(\mathbf{Y}) = \frac{5}{3}, \quad (4.4)$$

which constitutes the subcharacteristic condition for (4.1) to relax to an equilibrium as $\epsilon \downarrow 0$ [11]. The set of states for (4.1) is

$$\Omega^r = \{ \mathbf{w} \in \mathbb{R}^{n_s + n_d + d + 2} : \rho_{1 \leq \alpha \leq n_s} > 0, \mathbf{v} \in \mathbb{R}^d, e_r > 0, e_{1 \leq \beta \leq n_d}^v > 0, e_s > 0 \}. \quad (4.5)$$

Let $\mathbf{w} = \lim_{\epsilon \downarrow 0} \mathbf{w}^\epsilon$, in this limit, one formally recovers (2.1a) with

$$\mathbf{u} = \mathcal{L}\mathbf{w}, \quad \mathbf{w} = \mathcal{M}(\mathbf{u}), \quad \mathbf{f}(\mathbf{u}) = \mathcal{L}\mathbf{g}(\mathcal{P}(\mathbf{u})), \quad (4.6)$$

with the operators $\mathcal{L} : \Omega^r \rightarrow \Omega^a$ and $\mathcal{P} : \Omega^a \rightarrow \Omega^r$ defined by

$$\mathcal{L}\mathbf{w} = (\boldsymbol{\rho}^\top, \rho \mathbf{v}^\top, \rho E_r + \rho e_s + \rho h_0 + \rho e_v, \rho \mathbf{e}_v^\top)^\top, \quad (4.7a)$$

$$\mathcal{P}(\mathbf{u}) = (\boldsymbol{\rho}^\top, \rho \mathbf{v}^\top, \rho e_r(\rho, p) + \rho e_c, \rho \mathbf{e}_v^\top, \rho(e_t - e_r(\rho, p)))^\top, \quad (4.7b)$$

with $e_r(\rho, p_r)$ defined from (4.2), $\rho = \sum_{\alpha=1}^{n_s} \rho_\alpha$, and $p = p(\mathbf{Y}, \rho, e_t)$ defined from (2.8). The equilibrium (4.6) corresponds to

$$E = E_r + e_s + h_0 + e_v, \quad e_t = e_r + e_s, \quad e_s = F(\mathbf{Y}, e_r) := \frac{\gamma - \gamma(\mathbf{Y})}{\gamma(\mathbf{Y}) - 1} e_r, \quad (4.8)$$

where the expression for F follows from the consistency relation on the pressure:

$$p(\mathbf{Y}, \rho, e_r + F(\mathbf{Y}, e_r)) \stackrel{(2.8)}{\stackrel{(4.2)}{=}} (\gamma(\mathbf{Y}) - 1) \rho (e_r + F(\mathbf{Y}, e_r)) = (\gamma - 1) \rho e_r. \quad (4.9)$$

4.2 Entropy

Let define the convex function

$$s_r(\tau, e_r) = -(\tau^{\gamma-1} e_r)^{\frac{1}{\gamma}}, \quad (4.10)$$

with $\tau = \frac{1}{\rho}$ the covolume of the mixture, and further introduce

$$\zeta(\mathcal{Y}, \tau, e_r, e_s, \mathbf{e}_v) = -s(\mathbf{Y}(\mathcal{Y}), \mathcal{T}(\mathcal{Y}, s_r(\tau, e_r), e_s), \mathcal{E}(\mathcal{Y}, e_s) + e_s, \mathbf{e}_v), \quad (4.11a)$$

$$\mathcal{E}(\mathcal{Y}, e_s) = \frac{\gamma(\mathbf{Y}) - 1}{\gamma - \gamma(\mathbf{Y})} e_s, \quad \mathcal{T}(\mathcal{Y}, s_r, e_s) = \left(\frac{\gamma - \gamma(\mathbf{Y})}{\gamma(\mathbf{Y}) - 1} \frac{(-s_r)^\gamma}{e_s} \right)^{\frac{1}{\gamma-1}}, \quad \mathbf{Y} = \mathbf{Y}(\mathcal{Y}), \quad (4.11b)$$

where s is the mixture entropy (2.19) for (2.1a) and

$$\mathcal{Y} = (Y_1, \dots, Y_{n_s-1})^\top \quad (4.12)$$

the vector of the mass fractions of the $n_s - 1$ first species. This particular change of variables will be used only in the proof of lemma 4.3 below where we will clarify the choice for n_s . Note that the mapping between $\mathbf{Y} = \mathbf{Y}(\mathcal{Y})$ is obviously one-to-one from (2.5) and (4.3) which is always satisfied for \mathbf{w} in Ω^r in (4.5), so we may adopt equivalently the notations \mathbf{Y} or \mathcal{Y} for the sake of clarity and write

$$r(\mathbf{Y}) = r(\mathcal{Y}) = r_{n_s} + \sum_{\alpha=1}^{n_s-1} Y_\alpha (r_\alpha - r_{n_s}). \quad (4.13)$$

In (4.11b), the function \mathcal{E} solves $e_s = F(\mathbf{Y}, e_r)$ for e_r with F defined in (4.8), while \mathcal{T} solves $s_r = s_r(\tau, \mathcal{E}(\mathcal{Y}, e_s))$ for τ through (4.10). Using (2.19) and (4.11), we easily obtain

$$\zeta(\mathcal{Y}, \tau, e_r, e_s, \mathbf{e}_v) = -s(\mathbf{Y}(\mathcal{Y}), \tau, e_r + e_s, \mathbf{e}_v) + \varsigma(\mathcal{Y}, e_r, e_s), \quad (4.14a)$$

$$\varsigma(\mathcal{Y}, e_r, e_s) = C_{v_t}(\mathcal{Y}) \ln \left(\frac{\gamma - \gamma(\mathcal{Y})}{\gamma - 1} \frac{e_r + e_s}{e_s} \left(\frac{\gamma(\mathcal{Y}) - 1}{\gamma - \gamma(\mathcal{Y})} \frac{e_s}{e_r} \right)^{\frac{\gamma(\mathcal{Y}) - 1}{\gamma - 1}} \right), \quad (4.14b)$$

with partial derivatives

$$\partial_\tau \zeta = -\frac{r(\mathcal{Y})}{\tau}, \quad \partial_{e_r} \zeta = -\frac{r(\mathcal{Y})}{(\gamma - 1)e_r}, \quad \partial_{e_s} \zeta = \frac{\gamma(\mathcal{Y}) - \gamma}{\gamma - 1} \frac{C_{v_t}(\mathcal{Y})}{e_s}. \quad (4.15)$$

Likewise, the mapping $\mathbf{w} \mapsto (\mathcal{Y}, \tau, e_r, e_s, \mathbf{e}_v)$ is surjective in Ω^r , so we may rewrite $\zeta = \zeta(\mathbf{w})$ as a function of the arguments in (4.11a). This change of variables is also motivated by the following result which will be used to prove convexity of the entropy in lemma 4.2.

Lemma 4.1 *Given twice differentiable functions $f(\mathbf{w}) = \rho g(\mathcal{Y}, \tau, e_r, e_s, \mathbf{e}_v)$, f is strictly convex iff. g is strictly convex in Ω^r .*

Proof Convexity being invariant under linear maps, the convexity of f is equivalent to that of $f(\mathbf{w}) = f_1(\rho_1, \dots, \rho_{n_s-1}, \rho, \rho \mathbf{v}^\top, \rho E_r, \rho \mathbf{e}_v, \rho e_s)$. Then, it is a classical matter that the convexity of f_1 and f_2 with $f_1(\rho, \mathbf{y}) = \rho f_2(\frac{1}{\rho}, \frac{1}{\rho} \mathbf{y})$ are equivalent. Since $E_r = e_r - \frac{1}{2} \mathbf{v} \cdot \mathbf{v}$, the convexity of f is equivalent to the convexity of $\rho f_2(\mathcal{Y}, \tau, \mathbf{v}, E_r, e_s, \mathbf{e}_v) = \rho g(\mathcal{Y}, \tau, e_r, e_s, \mathbf{e}_v)$ [22, chap. 2]. \square

Lemma 4.2 *Under the assumption (4.4), the function $\rho \zeta(\mathbf{w})$ defined by (4.11) is a strictly convex entropy in Ω^r for (4.1).*

Proof This proof has been moved to appendix A for the sake of clarity. \square

4.3 Properties of the relaxation system close to equilibrium

We first prove the following variational principle which states that the equilibrium (4.8) minimizes the entropy ζ and constitutes an analogue to the Gibbs Lemma in kinetic theory.

Lemma 4.3 *Under the assumption (4.4), the function ζ defined by (4.11) satisfies the following variational principle:*

$$-s(\mathbf{Y}, \tau, e_t, \mathbf{e}_v) = \min_{e_r + e_s = e_t} \left\{ \zeta(\mathcal{Y}(\mathbf{Y}), \tau, e_r, e_s, \mathbf{e}_v) : \right. \\ \left. 0 < Y_{1 \leq \alpha \leq n_s} \leq 1, \tau > 0, e_r > 0, e_s > 0, e_{1 \leq \beta \leq n_d}^v > 0 \right\}, \quad (4.16)$$

and the minimum is reached at a unique global equilibrium which is solution to (4.8).

Proof Note that (4.16) corresponds to the minimization of a strictly convex function (see lemma 4.2) in the convex set (4.5) under the linear constraint $e_r + e_s = e_t$, so we only need to find a local minimum for ζ which satisfies (4.16). We further prove that ς in (4.14) is positive and vanishes at equilibrium (4.8) that constitutes a global minimum. Let us rewrite ς as $C_{v_t}(\mathcal{Y}) \ln(f(\alpha, x))$ with $f(\alpha, x) = \frac{(1-\alpha)(1+x)}{x} \left(\frac{\alpha x}{1-\alpha}\right)^\alpha$, $x = \frac{e_s}{e_r} > 0$, and $\alpha = \frac{\gamma(\mathcal{Y})-1}{\gamma-1}$ in $(0, 1)$ from (4.4). We have $\partial_x f(\alpha, x) = \frac{1-\alpha}{x^2}(\alpha x + \alpha - 1)$, thus $\partial_x f(\alpha, x) < 0$ for $0 < x < x_{min} := \frac{1-\alpha}{\alpha}$, $\partial_x f(\alpha, x) > 0$ for $x > x_{min}$, and $\partial_x f(\alpha, x_{min}) = 0$. Since $f(\alpha, x_{min}) = 1$, ς vanishes at the global minimum $\alpha x_{min} = 1 - \alpha \Leftrightarrow \frac{\gamma(\mathcal{Y})-1}{\gamma-1} \frac{e_s}{e_r} = 1 - \frac{\gamma(\mathcal{Y})-1}{\gamma-1}$ which indeed corresponds to the equilibrium (4.8): $e_s = F(\mathcal{Y}, e_r)$. \square

The next result concerns the spatially homogeneous system in (4.1):

$$\partial_t \mathbf{w}^\epsilon = -\frac{1}{\epsilon} (\mathbf{w}^\epsilon - \mathcal{M}(\mathbf{w}^\epsilon)), \quad (4.17)$$

and is analogue to the H-theorem for kinetic equations. The result below shows that in the limit of instantaneous relaxation $\epsilon \downarrow 0$ the solution to (4.1) will converge to the equilibrium (4.8).

Theorem 4.1 *The vector of variables $\mathbf{u} = (\rho^\top, \rho \mathbf{v}^\top, \rho E, \rho \mathbf{e}_v^\top)^\top$ with $E = E_r + e_s + h_0 + e_v$ is a constant of (4.17) and the entropy $\rho \zeta$ decreases in time and reaches a unique minimum which corresponds to the equilibrium (4.8). This equilibrium is stable in the sense of Lyapunov.*

Proof From (4.17), we directly obtain that ρ , $\rho \mathbf{v}$, and $\rho \mathbf{e}_v$ are constant so $\partial_t(\rho \mathbf{e}_v) = 0$ and $\partial_t \mathbf{Y} = 0$. Then summing the ρE_r and ρe_s equations gives $\partial_t(\rho E_r + \rho e_s) = 0$ so \mathbf{u} in theorem 4.1 is constant.

Then, for smooth solutions of (4.17) we get

$$\begin{aligned} \partial_t \zeta(\mathbf{Y}^\epsilon, \tau^\epsilon, e_r^\epsilon, e_s^\epsilon) &= -\tau^{\epsilon^2} \partial_\tau \zeta \partial_t \rho^\epsilon + \partial_{e_r} \zeta \partial_t e_r^\epsilon + \partial_{e_s} \zeta \partial_t e_s^\epsilon \\ &= \frac{1}{\epsilon} (e_s^\epsilon - F(\mathcal{Y}^\epsilon, e_r^\epsilon)) (\partial_{e_r} \zeta - \partial_{e_s} \zeta)^\epsilon \\ &\stackrel{(4.15)}{=} -\frac{1}{\epsilon} \frac{r(\mathcal{Y}^\epsilon)}{(\gamma-1)e_r^\epsilon e_s^\epsilon} (e_s^\epsilon - F(\mathcal{Y}^\epsilon, e_r^\epsilon))^2 \leq 0, \end{aligned}$$

so $\partial_t \zeta \leq 0$ and $\partial_t \zeta = 0$ iff. $e_s^\epsilon = F(\mathcal{Y}^\epsilon, e_r^\epsilon)$ which corresponds to the equilibrium (4.8) which in turn corresponds to the global minimum of ζ from lemma 4.3. We therefore conclude that the system is stable by applying the Lyapunov stability criterion with the Lyapunov function $\mathbf{w} \mapsto \zeta(\mathbf{w} + \mathbf{w}^0) - \zeta(\mathbf{w}^0)$ where $\mathbf{w}^0 = \mathcal{P}(\mathbf{u})$ corresponds to the equilibrium (4.8) with \mathcal{P} defined in (4.7). Finally note that the partial energies are given explicitly by $e_\alpha^t = C_{v_\alpha}^t e_t / C_{v_t}(\mathbf{Y})$ which confirms that the equilibrium corresponds to a unique state. \square

The last result describes the first-order asymptotic analysis of small perturbations in the relaxation process in the neighborhood of the equilibrium (4.8) by performing a formal Chapman-Enskog expansion [5]. This result extends [11, Prop. 2.4] to multicomponent flows and allows to understand the relaxation process close to equilibrium as a viscous perturbation to (2.1a) and to prove well-posedness of (4.1) and consistency with (2.1a) when $\epsilon \downarrow 0$.

Theorem 4.2 *In the limit $\epsilon \downarrow 0$, small perturbations to the equilibrium (4.8) obey the following first order asymptotic expansion in ϵ :*

$$\partial_t \mathbf{u}^\epsilon + \nabla \cdot \mathbf{f}(\mathbf{u}^\epsilon) - \nabla \cdot \mathbf{f}_v(\mathbf{u}^\epsilon, \nabla \mathbf{u}^\epsilon) = 0, \quad \mathbf{f}_v(\mathbf{u}^\epsilon, \nabla \mathbf{u}^\epsilon) = \mu(\mathbf{Y}^\epsilon, \rho^\epsilon, e_t^\epsilon) \begin{pmatrix} 0 \\ (\nabla \cdot \mathbf{v}^\epsilon) \mathbf{I}_d \\ (\nabla \cdot \mathbf{v}^\epsilon) \mathbf{v}^{\epsilon \top} \\ 0 \end{pmatrix},$$

with $\mu(\mathbf{Y}^\epsilon, \rho^\epsilon, e_t^\epsilon) = \epsilon \frac{(\gamma - \gamma(\mathbf{Y}^\epsilon))(\gamma(\mathbf{Y}^\epsilon) - 1)^2}{\gamma - 1} \rho^\epsilon e_t^\epsilon$ positive under (4.4).

Proof Let consider perturbations to the equilibrium expanded in the form

$$e_r^\epsilon = e_r^0 + \epsilon e_r^1 + \epsilon^2 e_r^2 + \dots, \quad e_s^\epsilon = e_s^0 + \epsilon e_s^1 + \epsilon^2 e_s^2 + \dots \quad (4.18)$$

First observe that smooth solutions to (4.1) with (4.2) satisfy

$$\partial_t \mathbf{Y}^\epsilon + \mathbf{v}^\epsilon \cdot \nabla \mathbf{Y}^\epsilon = 0, \quad (4.19a)$$

$$\partial_t e_r^\epsilon + \mathbf{v}^\epsilon \cdot \nabla e_r^\epsilon + (\gamma - 1) e_r^\epsilon \nabla \cdot \mathbf{v}^\epsilon = \frac{e_s^\epsilon - F(\mathbf{Y}^\epsilon, e_r^\epsilon)}{\epsilon}, \quad (4.19b)$$

$$\partial_t e_s^\epsilon + \mathbf{v}^\epsilon \cdot \nabla e_s^\epsilon = -\frac{e_s^\epsilon - F(\mathbf{Y}^\epsilon, e_r^\epsilon)}{\epsilon}, \quad (4.19c)$$

from which we deduce

$$\partial_t F(\mathbf{Y}^\epsilon, e_r^\epsilon) + \mathbf{v}^\epsilon \cdot \nabla F(\mathbf{Y}^\epsilon, e_r^\epsilon) = \frac{\gamma - \gamma(\mathbf{Y}^\epsilon)}{\gamma(\mathbf{Y}^\epsilon) - 1} \left(\frac{e_s^\epsilon - F(\mathbf{Y}^\epsilon, e_r^\epsilon)}{\epsilon} - (\gamma - 1) e_r^\epsilon \nabla \cdot \mathbf{v}^\epsilon \right). \quad (4.20)$$

Plugging (4.18) into either (4.19b), or (4.19c), the order $\mathcal{O}(\epsilon^{-1})$ imposes

$$e_s^0 = F(\mathbf{Y}^\epsilon, e_r^0) = \frac{\gamma - \gamma(\mathbf{Y}^\epsilon)}{\gamma(\mathbf{Y}^\epsilon) - 1} e_r^0,$$

while the constraint $e_t^\epsilon = e_r^\epsilon + e_s^\epsilon = e_r^0 + F(\mathbf{Y}^\epsilon, e_r^0)$ in (4.16) gives

$$e_r^0 = \frac{\gamma(\mathbf{Y}^\epsilon) - 1}{\gamma - 1} e_t^\epsilon, \quad e_s^0 = \frac{\gamma - \gamma(\mathbf{Y}^\epsilon)}{\gamma - 1} e_t^\epsilon, \quad e_r^k + e_s^k = 0 \quad \forall k \geq 1.$$

Plugging again (4.18) into (4.19c) and (4.20), we obtain at leading order

$$\partial_t e_s^0 + \mathbf{v}^\epsilon \cdot \nabla e_s^0 = -(e_s^1 - F(\mathbf{Y}^\epsilon, e_r^1)),$$

$$\partial_t F(\mathbf{Y}^\epsilon, e_r^0) + \mathbf{v}^\epsilon \cdot \nabla F(\mathbf{Y}^\epsilon, e_r^0) = \frac{\gamma - \gamma(\mathbf{Y}^\epsilon)}{\gamma(\mathbf{Y}^\epsilon) - 1} \left(e_s^1 - F(\mathbf{Y}^\epsilon, e_r^1) - (\gamma - 1) e_r^0 \nabla \cdot \mathbf{v}^\epsilon \right),$$

and since $e_s^0 = F(\mathbf{Y}^\epsilon, e_r^0)$, we get

$$-(e_s^1 - F(\mathbf{Y}^\epsilon, e_r^1)) = \frac{\gamma - \gamma(\mathbf{Y}^\epsilon)}{\gamma(\mathbf{Y}^\epsilon) - 1} \left(e_s^1 - F(\mathbf{Y}^\epsilon, e_r^1) - (\gamma - 1) e_r^0 \nabla \cdot \mathbf{v}^\epsilon \right),$$

and using the above expressions for e_r^0 and e_s^0 gives

$$e_r^1 = -e_s^1 = -(\gamma - \gamma(\mathbf{Y}^\epsilon)) \left(\frac{\gamma(\mathbf{Y}^\epsilon) - 1}{\gamma - 1} \right)^2 e_t^\epsilon \nabla \cdot \mathbf{v}^\epsilon.$$

Finally, in (4.1) consider the momentum equation and add up the equations for ρE_r , ρe_s , ρe_v together with an equation for $\rho h_0 = \sum_\alpha \rho_\alpha h_\alpha^0$. We then obtain up to order $\mathcal{O}(\epsilon)$

$$\begin{aligned} \partial_t \rho^\epsilon \mathbf{v}^\epsilon + \nabla \cdot (\rho^\epsilon \mathbf{v}^\epsilon \mathbf{v}^{\epsilon\top} + p_r(\rho^\epsilon, e_r^0 + \epsilon e_r^1)) &= 0, \\ \partial_t \rho^\epsilon E^\epsilon + \nabla \cdot \left((\rho^\epsilon E^\epsilon + p_r(\rho^\epsilon, e_r^0 + \epsilon e_r^1)) \mathbf{v}^\epsilon \right) &= 0, \end{aligned}$$

and we conclude by observing that $p_r(\rho^\epsilon, e_r^0) = p(\mathbf{Y}^\epsilon, \rho^\epsilon, e_t^\epsilon)$ from (4.9) and by using the expression for e_r^1 . \square

4.4 General framework for the design of three-point schemes

We now clarify the form of the numerical flux for (2.1a) that we deduce from a numerical flux for (4.1) in homogeneous form. The former flux will satisfy the properties (i) to (vi) in section 3 providing that the latter satisfies similar properties. The three-point scheme for (4.1) $_{\epsilon \rightarrow \infty}$ reads

$$\mathbf{W}_j^{n+1} - \mathbf{W}_j^n + \frac{\Delta t^{(n)}}{\Delta x} (\mathbf{H}(\mathbf{W}_j^n, \mathbf{W}_{j+1}^n, \mathbf{n}) - \mathbf{H}(\mathbf{W}_{j-1}^n, \mathbf{W}_j^n, \mathbf{n})) = 0, \quad (4.21)$$

with $\mathbf{H}(\mathbf{w}, \mathbf{w}, \mathbf{n}) = \mathbf{g}(\mathbf{w}) \cdot \mathbf{n}$. We assume that under some CFL condition on the time step (see section 5), (4.21) enjoys the properties (i) to (vi) in section 3. In particular we have

$$\rho \zeta(\mathbf{W}_j^{n+1}) \leq \rho \zeta(\mathbf{W}_j^n) - \frac{\Delta t^{(n)}}{\Delta x} (Z(\mathbf{W}_j^n, \mathbf{W}_{j+1}^n, \mathbf{n}) - Z(\mathbf{W}_{j-1}^n, \mathbf{W}_j^n, \mathbf{n})), \quad (4.22)$$

with $Z(\mathbf{w}, \mathbf{w}, \mathbf{n}) = \rho \zeta \mathbf{v} \cdot \mathbf{n}$. Then, from (4.21) we may design a scheme for (2.1a) as stated in the theorem below.

Theorem 4.3 *Consider the three-point numerical scheme (4.21) for (4.1) $_{\epsilon \rightarrow \infty}$, i.e., $\epsilon \rightarrow \infty$ in (4.1), with Lipschitz, consistent and conservative numerical flux. Assume that it satisfies (4.22) with a consistent numerical flux, some maximum principle on the mass fractions*

$$\min(Y_{\alpha_{j-1}}^n, Y_{\alpha_j}^n, Y_{\alpha_{j+1}}^n) \leq Y_{\alpha_j}^{n+1} \leq \max(Y_{\alpha_{j-1}}^n, Y_{\alpha_j}^n, Y_{\alpha_{j+1}}^n) \quad \forall 1 \leq \alpha \leq n_s, \quad (4.23)$$

and the specific entropy

$$\zeta(\mathbf{W}_j^{n+1}) \leq \max(\zeta(\mathbf{W}_{j-1}^n), \zeta(\mathbf{W}_j^n), \zeta(\mathbf{W}_{j+1}^n)), \quad (4.24)$$

and is robust, $\mathbf{W}_{j \in \mathbb{Z}}^{n \geq 0} \in \Omega^r$. If (4.4) holds, the three-point numerical scheme (3.2) with the Lipschitz, consistent and conservative numerical flux

$$\begin{aligned} \mathbf{h}(\mathbf{u}^-, \mathbf{u}^+, \mathbf{n}) &= \mathcal{LH}(\mathcal{P}(\mathbf{u}^-), \mathcal{P}(\mathbf{u}^+), \mathbf{n}), \quad (4.25) \\ h_X(\mathbf{u}^-, \mathbf{u}^+, \mathbf{n}) &= H_X(\mathcal{P}(\mathbf{u}^-), \mathcal{P}(\mathbf{u}^+), \mathbf{n}), \quad X \in \{\rho, \rho \mathbf{v}, \rho \mathbf{e}_v\}, \\ h_{\rho E}(\mathbf{u}^-, \mathbf{u}^+, \mathbf{n}) &= H_{\rho E_r}(\mathcal{P}(\mathbf{u}^-), \mathcal{P}(\mathbf{u}^+), \mathbf{n}) + H_{\rho e_s}(\mathcal{P}(\mathbf{u}^-), \mathcal{P}(\mathbf{u}^+), \mathbf{n}) \\ &\quad + \sum_{\alpha=1}^{n_s} h_\alpha^0 H_{\rho_\alpha}(\mathcal{P}(\mathbf{u}^-), \mathcal{P}(\mathbf{u}^+), \mathbf{n}) + \sum_{\beta=1}^{n_d} H_{\rho e_\beta^v}(\mathcal{P}(\mathbf{u}^-), \mathcal{P}(\mathbf{u}^+), \mathbf{n}), \end{aligned}$$

with \mathcal{L} defined in (4.7), is ES for the pair (η, \mathbf{q}) in (2.13), satisfies (3.6) with $Q(\mathbf{u}^-, \mathbf{u}^+, \mathbf{n}) = Z(\mathcal{P}(\mathbf{u}^-), \mathcal{P}(\mathbf{u}^+), \mathbf{n})$, the minimum and maximum principles (3.7) and (3.8), and is robust, $\mathbf{U}_j^{n \geq 0} \in \Omega^a$.

Proof By consistency of \mathbf{H} : $\mathbf{h}(\mathbf{u}, \mathbf{u}, \mathbf{n}) \stackrel{(4.25)}{=} \mathcal{L}\mathbf{H}(\mathcal{P}(\mathbf{u}), \mathcal{P}(\mathbf{u}), \mathbf{n}) = \mathcal{L}\mathbf{g}(\mathcal{P}(\mathbf{u})) \cdot \mathbf{n} \stackrel{(4.6)}{=} \mathbf{f}(\mathbf{u}) \cdot \mathbf{n}$, while Lipschitz continuity and conservation are direct since \mathcal{L} is linear.

Then, let $\mathbf{W}_j^n = \mathcal{P}(\mathbf{U}_j^n)$ so $\rho\zeta(\mathbf{W}_j^n) = \eta(\mathbf{U}_j^n)$ and $Z(\mathbf{W}_j^n, \mathbf{W}_{j+1}^n, \mathbf{n}) = Q(\mathbf{U}_j^n, \mathbf{U}_{j+1}^n, \mathbf{n})$, and define \mathbf{W}_j^{n+1} from (4.21) and $\mathbf{U}_j^{n+1} = \mathcal{L}\mathbf{W}_j^{n+1}$. If $\mathbf{U}_j^n \in \Omega^a$, then $\mathbf{W}_j^n = \mathcal{P}(\mathbf{U}_j^n) \in \Omega^r$ since $e_r = \frac{\gamma(\mathbf{Y})-1}{\gamma-1}e_t$ and $e_s = \frac{\gamma-\gamma(\mathbf{Y})}{\gamma-1}e_t$, and $\mathbf{W}_j^{n+1} \in \Omega^r$ so $\mathbf{U}_j^{n+1} = \mathcal{L}\mathbf{W}_j^{n+1} \in \Omega^a$ by (4.6). Now, by the variational principle (4.16) we have

$$\begin{aligned} \eta(\mathbf{U}_j^{n+1}) &\stackrel{(4.16)}{\leq} \rho\zeta(\mathbf{W}_j^{n+1}) \\ &\stackrel{(4.22)}{\leq} \rho\zeta(\mathbf{W}_j^n) - \frac{\Delta t^{(n)}}{\Delta x} (Z(\mathbf{W}_j^n, \mathbf{W}_{j+1}^n, \mathbf{n}) - Z(\mathbf{W}_{j-1}^n, \mathbf{W}_j^n, \mathbf{n})) \\ &= \rho\zeta(\mathcal{P}(\mathbf{U}_j^n)) - \frac{\Delta t^{(n)}}{\Delta x} (Z(\mathcal{P}(\mathbf{U}_j^n), \mathcal{P}(\mathbf{U}_{j+1}^n), \mathbf{n}) - Z(\mathcal{P}(\mathbf{U}_{j-1}^n), \mathcal{P}(\mathbf{U}_j^n), \mathbf{n})) \\ &= \eta(\mathbf{U}_j^n) - \frac{\Delta t^{(n)}}{\Delta x} (Q(\mathbf{U}_j^n, \mathbf{U}_{j+1}^n, \mathbf{n}) - Q(\mathbf{U}_{j-1}^n, \mathbf{U}_j^n, \mathbf{n})). \end{aligned}$$

Finally, plugging $\zeta(\mathbf{W}_j^n) = -s(\mathbf{U}_j^n)$ into (4.24) for all j and using (4.16) we obtain (3.8), while (3.7) holds because (4.23) and the components associated to $\boldsymbol{\rho}$ in (4.25) remain unaffected. \square

Since the pressure in (4.1) obeys a polytropic ideal gas EOS and the variables $(\mathbf{Y}, \mathbf{e}_v, e_s)$ are purely advected, one may use many methods for (4.21) such as, e.g., the Godunov [23], Rusanov [44], HLL [27], or Roe [42] schemes, though the latter method does not guaranty robustness [16]. In the next section we will consider some of these schemes.

In the definition of the numerical flux (4.25), the \mathcal{L} operator consists in adding up some components of \mathbf{H} to build the numerical flux for the total energy, ρE , while the \mathcal{P} operators consist in taking data at equilibrium. This last operation is equivalent to applying instantaneous relaxation, i.e., to consider $(4.1)_{\epsilon \rightarrow \infty}$, through a splitting of hyperbolic and relaxation operators [11]. Note that instantaneous relaxation is here justified by the analysis in section 4.3. This approach is also in agreement with the numerical flux we will consider that uses discrete projections onto Maxwellian equilibria [3].

Remark 4.1 We note that theorem 4.3 may be directly applied to the multidimensional schemes (3.1) instead of the three-point scheme (3.2). This may allow to use genuinely multi-dimensional schemes possibly with a less restrictive constraint on the time step. In contrast considering (3.2) with the CFL condition (3.9) would allow to encompass more general schemes such as the ARS we will consider in section 5.

5 Examples of three-point schemes

In this section we consider examples of three-point schemes (4.21) for the homogeneous energy relaxation system $(4.1)_{\epsilon \rightarrow \infty}$ to illustrate theorem 4.3. Such schemes

define schemes (3.2) for (2.1a) through (4.25). As already noticed, other numerical schemes may be used since we use a simple polytropic EOS in (4.1).

The schemes we consider use Riemann type solvers with numerical flux in (4.21) of the form

$$\mathbf{H}(\mathbf{w}^-, \mathbf{w}^+, \mathbf{n}) = \mathbf{g}(\mathcal{W}(0; \mathbf{w}^-, \mathbf{w}^+, \mathbf{n})) \cdot \mathbf{n}, \quad (5.1)$$

where $\mathcal{W}(\cdot; \mathbf{w}_L, \mathbf{w}_R, \mathbf{n})$ is used to approximate the solution to the Riemann problem (4.1) $_{\epsilon \rightarrow \infty}$ with initial data $\mathbf{w}_0(x) = \mathbf{w}_L$ if $x := \mathbf{x} \cdot \mathbf{n} < 0$ and $\mathbf{w}_0(x) = \mathbf{w}_R$ if $\mathbf{x} \cdot \mathbf{n} > 0$. We then build three-point schemes for (2.1a) by simply applying (4.25).

5.1 The Godunov method

As noticed in [11] it is possible to apply the exact Riemann solver [23] for polytropic gas to (4.21) where \mathcal{W} corresponds to the exact entropy weak solution to the Riemann problem. Consider the compressible Euler equations

$$\partial_t \tilde{\mathbf{w}} + \nabla \cdot \tilde{\mathbf{g}}(\tilde{\mathbf{w}}) = 0, \quad \tilde{\mathbf{w}} = \begin{pmatrix} \rho \\ \rho \mathbf{v} \\ \rho E_r \end{pmatrix}, \quad \tilde{\mathbf{g}}(\tilde{\mathbf{w}}) = \begin{pmatrix} \rho \mathbf{v}^\top \\ \rho \mathbf{v} \mathbf{v}^\top + p_r \mathbf{I} \\ (\rho E_r + p_r) \mathbf{v}^\top \end{pmatrix}, \quad (5.2)$$

with p_r defined from (4.2) and γ satisfying (4.4).

Any variable ψ in $\{\mathbf{Y}, \mathbf{e}_v, e_s\}$ is uncoupled from the $\tilde{\mathbf{w}}$ variables and is only purely transported in (4.1) $_{\epsilon \rightarrow \infty}$. Noting that the intermediate states are $(\psi_L, \psi_L, \psi_R, \psi_R)$, the entropy weak solution is made of the Riemann solution for the Euler equations with variables $\tilde{\mathbf{w}}$ and fluxes $\tilde{\mathbf{g}}(\tilde{\mathbf{w}})$ plus the states for ψ [11, Lemma 4.6]. The Godunov method is thus ES and guaranties robustness of (4.21) as well as the minimum and maximum principles (4.23) and (4.24) under some standard CFL condition.

Let $\rho, u = \mathbf{v} \cdot \mathbf{n}$ and p_r be the solution to the Riemann problem for (5.2) with initial data $\tilde{\mathbf{w}}_0(x) = (\rho_L, u_L, p(\mathbf{Y}_L, \rho_L, e_{t_L}))^\top$ if $x := \mathbf{x} \cdot \mathbf{n} < 0$ and $\tilde{\mathbf{w}}_0(x) = (\rho_R, u_R, p(\mathbf{Y}_R, \rho_R, e_{t_R}))^\top$ if $\mathbf{x} \cdot \mathbf{n} > 0$ and let u^* be the velocity in the star region. Note that $p_{r_X} = p_X$ given by (2.8) for $X = L, R$ since data are taken at equilibrium in (4.25). Then the numerical flux for (3.2) reads

$$\mathbf{h}^{God}(\mathbf{u}_L, \mathbf{u}_R, \mathbf{n}) = \begin{pmatrix} \rho(\epsilon_L \mathbf{Y}_L + \epsilon_R \mathbf{Y}_R)u \\ \rho u(\mathbf{u} \mathbf{n} + \epsilon_L \mathbf{v}_L^\perp + \epsilon_R \mathbf{v}_R^\perp) + p_r \mathbf{n} \\ \rho(\epsilon_L E_L^* + \epsilon_R E_R^*)u + p_r u \\ \rho(\epsilon_L e_{v_L} + \epsilon_R e_{v_R})u \end{pmatrix}, \quad (5.3)$$

where $E_X^* = h_0(\mathbf{Y}_X) + e_r + \frac{\gamma - \gamma(\mathbf{Y}_X)}{\gamma(\mathbf{Y}_X) - 1} e_r + e_{v_X} + \frac{\mathbf{v}_X^\perp \cdot \mathbf{v}_X^\perp + u^2}{2}$, $e_r = \frac{p_r}{(\gamma - 1)\rho}$, $\mathbf{v}_X^\perp = \mathbf{v}_X - (\mathbf{v}_X \cdot \mathbf{n})\mathbf{n}$, $X = L, R$, $\epsilon_L = 1$ if $u^* > 0$ and 0 else, and $\epsilon_R = 1 - \epsilon_L$. Finally, the condition on the time step is (3.3) with $\lambda(\mathbf{u}) = |\mathbf{v} \cdot \mathbf{n}| + c_\gamma(\rho, p)$ with $c_\gamma(\rho, p) = \sqrt{\gamma p / \rho}$ and p defined from (2.8).

5.2 The HLL numerical flux

The HLL approximate Riemann solver [27] for (4.21) reads

$$\mathcal{W}^{hll}(\mathbf{w}_L, \mathbf{w}_R, \mathbf{n}) = \begin{cases} \mathbf{w}_L, & \frac{x}{t} < S_L, \\ \frac{S_R \mathbf{w}_R - S_L \mathbf{w}_L + \mathbf{g}(\mathbf{w}_L) - \mathbf{g}(\mathbf{w}_R)}{S_R - S_L}, & S_L < \frac{x}{t} < S_R, \\ \mathbf{w}_R, & S_R < \frac{x}{t}, \end{cases} \quad (5.4)$$

and is ES [27] and robust [16] under the CFL condition (3.3), with $\lambda = \max(|S_L|, |S_R|)$, providing that S_L (resp. S_R) is a lower (resp. upper) bound of the speed of the leftmost (resp. rightmost) wave in the exact Riemann solution. Applying (4.25), the numerical flux for (3.2) reads

$$\mathbf{h}^{hll}(\mathbf{u}_L, \mathbf{u}_R, \mathbf{n}) = \begin{cases} \mathbf{f}(\mathbf{u}_L) \cdot \mathbf{n}, & \frac{x}{t} < S_L, \\ \frac{S_R \mathbf{f}(\mathbf{u}_L) \cdot \mathbf{n} - S_L \mathbf{f}(\mathbf{u}_R) \cdot \mathbf{n} + S_L S_R (\mathbf{u}_R - \mathbf{u}_L)}{S_R - S_L}, & S_L < \frac{x}{t} < S_R, \\ \mathbf{f}(\mathbf{u}_R) \cdot \mathbf{n}, & S_R < \frac{x}{t}, \end{cases} \quad (5.5)$$

and we evaluate the wave speeds from the two-rarefaction approximation [51, Ch. 9]:

$$S_L = \mathbf{v}_L \cdot \mathbf{n} - c_L, \quad S_R = \mathbf{v}_R \cdot \mathbf{n} + c_R, \quad c_X = c_\gamma(\rho_X, p_X) \sqrt{1 + \frac{\gamma+1}{2\gamma} \left(\frac{p_{tr}^*}{p_X} - 1 \right)^+},$$

where $(\cdot)^+ = \max(\cdot, 0)$ denotes the positive part, $c_\gamma(\rho, p) = \sqrt{\gamma p / \rho}$, $p_X = p(\mathbf{Y}_X, \rho_X, e_{t_X})$ given by (2.8), γ satisfying (4.4), and

$$p_{tr}^* = \left(\frac{c_\gamma(\rho_L, p_L) + c_\gamma(\rho_R, p_R) + \frac{\gamma-1}{2} (\mathbf{v}_L - \mathbf{v}_R) \cdot \mathbf{n}}{c_\gamma(\rho_L, p_L) p_L^{-\frac{\gamma-1}{2\gamma}} + c_\gamma(\rho_R, p_R) p_R^{-\frac{\gamma-1}{2\gamma}}} \right)^{\frac{2\gamma}{\gamma-1}}.$$

Note that the two-rarefaction approximation holds for the compressible Euler equations with a polytropic EOS for an adiabatic exponent $1 < \gamma \leq \frac{5}{3}$ [25]. The strict inequality in (4.4) may thus prevent the bound estimates with this approach. However, the analysis in [25, Lemma 4.2] shows that this may occur only for moderate shock strengths so the scheme remains ES for strong shocks as expected in practice. For instance, we use $\gamma = 1.01 \times \frac{5}{3}$ in the numerical experiments of section 6 for which the above estimates are valid when either $p_{tr}^* \leq p_X$, or $p_{tr}^* \gtrsim 1.05 p_X$.

5.3 Pressure relaxation-based numerical flux

We now consider the numerical flux based on relaxation of pressure [3, Prop. 2.21]. The approximate Riemann solver for (4.21) reads

$$\mathcal{W}^r\left(\frac{x}{t}; \mathbf{w}_L, \mathbf{w}_R, \mathbf{n}\right) = \begin{cases} \mathbf{w}_L, & \frac{x}{t} < S_L, \\ \mathbf{w}_L^*, & S_L < \frac{x}{t} < u^*, \\ \mathbf{w}_R^*, & u^* < \frac{x}{t} < S_R, \\ \mathbf{w}_R, & S_R < \frac{x}{t}, \end{cases} \quad (5.6)$$

where $\mathbf{w}_X^* = (\rho_X^* \mathbf{Y}_X^\top, \rho_X^* \mathbf{v}_X^{*\top}, \rho_X^* E_{r,X}^*, \rho_X^* \mathbf{e}_{v,X}^\top, \rho_X^* e_{s,X})^\top$, for $X = L, R$, and

$$\mathbf{v}_L^* = \mathbf{v}_L^\perp + u^* \mathbf{n}, \quad \mathbf{v}_R^* = \mathbf{v}_R^\perp + u^* \mathbf{n}, \quad (5.7a)$$

$$u^* = \frac{a_L u_L + a_R u_R + p_{r,L} - p_{r,R}}{a_L + a_R}, \quad p^* = \frac{a_R p_{r,L} + a_L p_{r,R} + a_L a_R (u_L - u_R)}{a_L + a_R}, \quad (5.7b)$$

$$\frac{1}{\rho_L^*} = \frac{1}{\rho_L} + \frac{u^* - u_L}{a_L}, \quad \frac{1}{\rho_R^*} = \frac{1}{\rho_R} + \frac{u_R - u^*}{a_R}, \quad (5.7c)$$

$$E_{r,L}^* = E_{r,L} - \frac{p^* u^* - p_{r,L} u_L}{a_L}, \quad E_{r,R}^* = E_{r,R} - \frac{p_{r,R} u_R - p^* u^*}{a_R}, \quad (5.7d)$$

where $\mathbf{v}_X^\perp = \mathbf{v}_X - u_X \mathbf{n}$, $u_X = \mathbf{v}_X \cdot \mathbf{n}$, $\rho_X = \sum_{\alpha=1}^{n_s} \rho_{\alpha X}$, $\mathbf{Y}_X = \frac{1}{\rho_X} \boldsymbol{\rho}_X$, and $p_{r,X} = p_r(\rho_X, e_{r,X})$ defined by (4.2).

The wave speeds in (5.6) are evaluated from $S_L = u_L - a_L/\rho_L$ and $S_R = u_R + a_R/\rho_R$ where the approximate Lagrangian sound speeds [3] are defined by

$$\begin{cases} \frac{a_L}{\rho_L} = c_\gamma(\rho_L, p_{r,L}) + \frac{\gamma+1}{2} \left(\frac{p_{r,R} - p_{r,L}}{\rho_R c_\gamma(\rho_R, p_{r,R})} + u_L - u_R \right)^+, \\ \frac{a_R}{\rho_R} = c_\gamma(\rho_R, p_{r,R}) + \frac{\gamma+1}{2} \left(\frac{p_{r,L} - p_{r,R}}{a_L} + u_L - u_R \right)^+, \end{cases} \quad \text{if } p_{r,R} \geq p_{r,L}, \quad (5.8a)$$

$$\begin{cases} \frac{a_R}{\rho_R} = c_\gamma(\rho_R, p_{r,R}) + \frac{\gamma+1}{2} \left(\frac{p_{r,L} - p_{r,R}}{\rho_L c_\gamma(\rho_L, p_{r,L})} + u_L - u_R \right)^+, \\ \frac{a_L}{\rho_L} = c_\gamma(\rho_L, p_{r,L}) + \frac{\gamma+1}{2} \left(\frac{p_{r,R} - p_{r,L}}{a_R} + u_L - u_R \right)^+, \end{cases} \quad \text{else,} \quad (5.8b)$$

with γ defined from (4.4).

This numerical scheme is based on a relaxation approximation using evolution equations for a relaxation pressure in place of p_r and for a in (5.7) in place of the Lagrangian sound speed $\rho c_\gamma(\rho, p_r)$. The Riemann solution contains only linearly degenerate fields and (5.6) follows from projection of the initial data onto an equilibrium manifold. We refer to [3, Sec. 2.4] or [9] for complete introductions and in-depth analyses. In particular, the analysis in [3, Sec. 2.4] proves the ES, robustness and the minimum principle on entropy by reversing the roles of energy conservation and entropy inequality [8]. This technique also applies to the entropy $\rho \zeta(\mathbf{w})$ and we may consider $\rho E_r = \rho e_r(\mathbf{Y}, \tau, \zeta, e_s, \mathbf{e}_v) + \frac{1}{2} \mathbf{v} \cdot \mathbf{v}$ as an entropy for the system defined by conservation laws for $(\boldsymbol{\rho}^\top, \rho \mathbf{v}^\top, \rho \zeta, \rho \mathbf{e}_v, \rho e_s)^\top$. Indeed, the convexity of $E_r(\mathbf{Y}, \tau, \zeta, e_s, \mathbf{e}_v)$ is equivalent to the convexity of $\zeta(\mathbf{Y}, \tau, e_r, e_s, \mathbf{e}_v)$ since from (4.14) $\partial_{e_r} \zeta = -\frac{r(\mathbf{Y})}{(\gamma-1)e_r} < 0$ [22, chap. 2].

The Bouchut scheme guaranties positivity of ρ and e_r under the CFL condition (3.3) with $\lambda = \max(|S_L|, |S_R|)$. Positivity of $\boldsymbol{\rho} = \rho \mathbf{Y}$, e_s and e_v then follows by cell-averaging the Riemann solution (5.7). Likewise, the discrete minimum maximum principle (4.23) holds for the same reason. Applying (4.25), the numerical flux for (3.2) reads

$$\mathbf{h}^r(\mathbf{u}_L, \mathbf{u}_R, \mathbf{n}) = \begin{cases} \mathbf{f}(\mathbf{u}_L) \cdot \mathbf{n}, & \frac{x}{t} < S_L, \\ \mathbf{f}(\mathbf{u}_L^*) \cdot \mathbf{n}, & S_L < \frac{x}{t} < u^*, \\ \mathbf{f}(\mathbf{u}_R^*) \cdot \mathbf{n}, & u^* < \frac{x}{t} < S_R, \\ \mathbf{f}(\mathbf{u}_R) \cdot \mathbf{n}, & S_R < \frac{x}{t}, \end{cases} \quad (5.9)$$

with $\mathbf{u}_X^* = (\rho_X^* \mathbf{Y}_X^\top, \rho_X^* \mathbf{v}_X^{*\top}, \rho_X^* E_X^*, \rho_X^* \mathbf{e}_{v,X}^\top)^\top$, for $X = L, R$, and

$$u^* = \frac{a_L u_L + a_R u_R + p_L - p_R}{a_L + a_R}, \quad p^* = \frac{a_R p_L + a_L p_R + a_L a_R (u_L - u_R)}{a_L + a_R},$$

$$E_L^* = E_L - \frac{p^* u^* - p_L u_L}{a_L}, \quad E_R^* = E_R - \frac{p_R u_R - p^* u^*}{a_R},$$

$p_X = p(\mathbf{Y}_X, \rho_X, e_{t_X})$ for $X = L, R$, the other quantities being defined in (5.7) and the wave speed estimates are defined from (5.8) with $p_r = p$ from (4.25).

5.4 Wall boundary conditions

Let consider the case of an impermeability condition, $\mathbf{v} \cdot \mathbf{n} = 0$, at a wall $\Gamma_w \subset \partial\Omega_h$ which is commonly imposed through the use of mirror state $\mathbf{u}^+ = (\rho, -\rho \mathbf{v}^\top, \rho E, \rho \mathbf{e}_v^\top)^\top$. For elements κ adjacent to a wall, we modify (3.1) in the following way

$$\mathbf{U}_\kappa^{n+1} = \mathbf{U}_\kappa^n - \frac{\Delta t^{(n)}}{|\kappa|} \left(\sum_{e \in \partial\kappa \setminus \Gamma_w} |e| \mathbf{h}(\mathbf{U}_\kappa^n, \mathbf{U}_{\kappa_e}^n, \mathbf{n}_e) + \sum_{e \in \partial\kappa \cap \Gamma_w} |e| \mathbf{h}^r(0, \mathbf{U}_\kappa^n, \mathbf{U}_\kappa^{n+}, \mathbf{n}_e) \right),$$

where \mathbf{h} corresponds to one of the above numerical fluxes, \mathbf{h}^r is pressure relaxation-based flux (5.9), and the exponent $+$ denotes the mirror state. The above scheme still can be written as a convex combination of updates of three-point schemes (3.2) as in (3.10), so the entropy inequality (3.11) holds.

Using the mirror state we have from (5.7) that $a_L = a_R = a$, $p_L = p_R = p$ given by (2.8), $\mathbf{Y}_L = \mathbf{Y}_R = \mathbf{Y}$ so the left and right states have the same thermodynamics. We thus obtain $\mathbf{h}^r(0, \mathbf{u}, \mathbf{u}^+, \mathbf{n}) = (0, 0, p^* \mathbf{n}, 0, 0)^\top$ with $p^* = p + a \mathbf{v} \cdot \mathbf{n}$, and $a = \sqrt{\gamma(\mathbf{Y}) \rho p} + (\gamma(\mathbf{Y}) + 1) \rho (\mathbf{v} \cdot \mathbf{n})^+$. This boundary condition is consistent with the impermeability condition and enforces the pressure through the characteristic associated to the eigenvalue $\mathbf{v} \cdot \mathbf{n} + c(\mathbf{Y}, e_t)$.

Note that from theorem 4.3 the entropy flux vanishes at wall boundary interfaces since by $Q(\mathbf{u}, \mathbf{u}^+, \mathbf{n}) = Z(\mathcal{P}(\mathbf{u}), \mathcal{P}(\mathbf{u}^+), \mathbf{n}) = \eta(\mathbf{u}) \mathbf{v} \cdot \mathbf{n}$ evaluated at $\mathcal{W}^r(0; \mathcal{P}(\mathbf{u}), \mathcal{P}(\mathbf{u}^+), \mathbf{n})$ for which $\mathbf{v} \cdot \mathbf{n} = u^* = 0$. Assuming either compactly supported solutions, or using ES boundary conditions from [46] at far-field boundaries, we end with the following global estimate on the entropy:

$$\sum_{\kappa \in \Omega_h} |\kappa| \eta(\mathbf{U}_\kappa^{n+1}) \leq \sum_{\kappa \in \Omega_h} |\kappa| \eta(\mathbf{U}_\kappa^n) + C,$$

where C is a constant that depends on boundary data. Using the strict convexity of the entropy $\eta(\mathbf{u})$, one may use Dafermos' argument to prove L^2 stability of the solution [12] (see e.g. [46, Th. 2.6]).

6 Numerical experiments

In this section we present numerical experiments, obtained with the CFD code *Aghora* developed at ONERA [41], on problems in one and two space dimensions in order to illustrate the performance of the schemes derived in this work. We use $\gamma = 1.01 \times \frac{5}{3}$ in (5.3) to ensure the inequality in (4.4), while we set $\gamma = \frac{5}{3}$

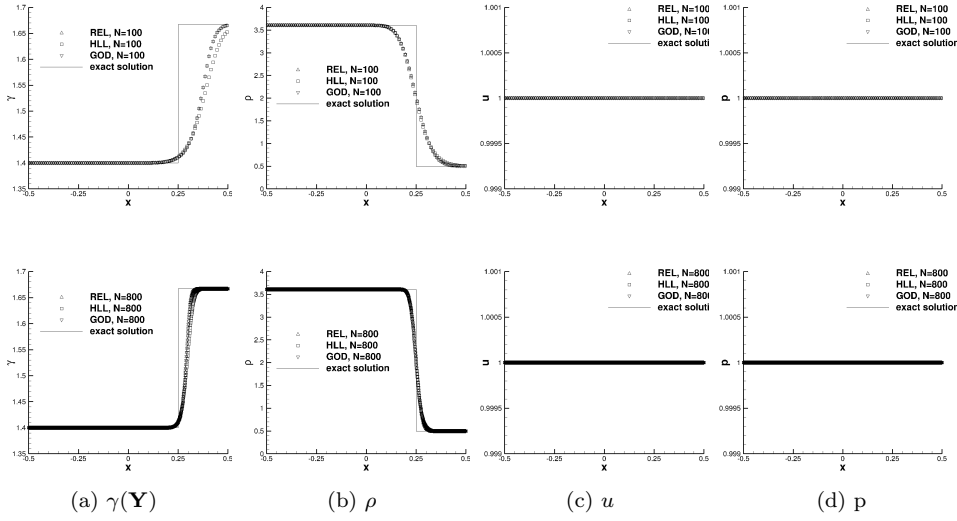


Fig. 6.1: Convection of a material interface: results obtained with the numerical fluxes (5.9) (REL), (5.5) (HLL), and (5.3) (GOD), on two grids with $N = 100$ and $N = 800$ elements.

in (5.8) and increase the wave speed estimates $S_{X=L,R}$ by a factor 1.01 in (5.5) and (5.9). The time step is evaluated through (3.3). For 2D simulations, we impose the freestream values at supersonic inlets and extrapolate variables at supersonic outlets, while we apply the impermeability boundary condition in section 5.4 at walls. Steady computations are obtained by using local time stepping until the ℓ^2 norm of the vector of residuals has decreased by a factor 10^{10} . Additional results obtained for a monocomponent perfect gas with an equivalent adiabatic exponent are also reported for the sake of comparison: we use either the Roe solver [42] with entropy fix [26] (referred to as ROE-PG), or the HLL solver [27] with the two-rarefaction approximation [51, Ch. 9] for computing the wave speeds (referred to as HLL-PG).

6.1 One-dimensional shock-tube problems

We first consider the convection of a material interface separating air ($\rho_L = 3.607655$, $Y_{1,L} = 1 - Y_{2,L} = 1$, $e_{v_1,L} = 1.8070291$, $\gamma_1 = 1.4$) in thermal disequilibrium from helium ($\rho_R = 0.5$, $Y_{1,R} = 1 - Y_{2,R} = 0$, $e_{v_1,R} = 0$, $\gamma_2 = \frac{5}{3}$) in a flow with pressure $p_L = p_R = 1$ and velocity $u_L = u_R = 1$. Results are shown in fig. 6.1 and highlight convergence of the three schemes with some more smearing of the contact by the HLL scheme as expected.

We now consider a shock tube problem adapted from [45] initially separating regions with large pressure and temperature ratios: $u_L = u_R = 0$, $p_L = 100p_R = 100\text{bars}$, and $T_L = 30T_R = 9000\text{K}$. We consider air in thermal equilibrium with

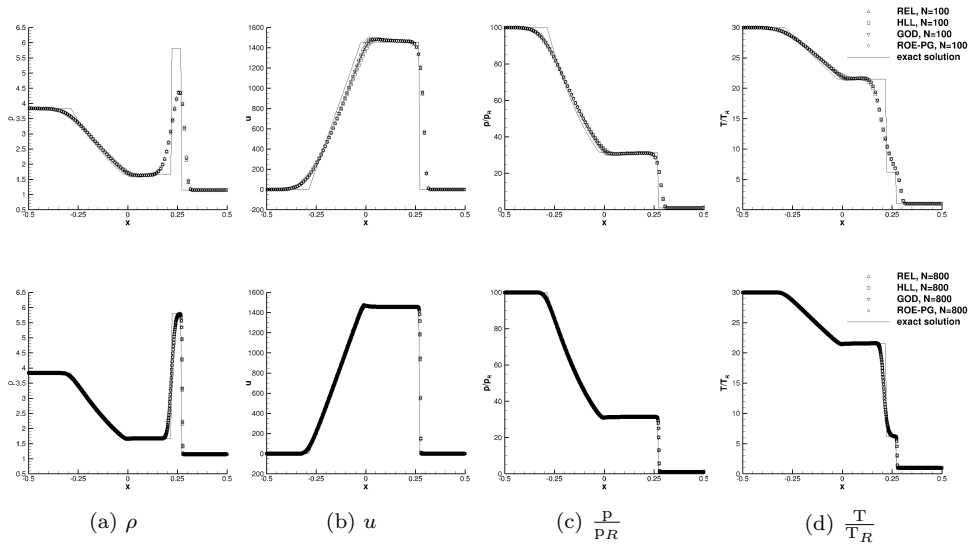


Fig. 6.2: Shock tube filled with air: results at time $t = 1.5 \times 10^{-4}$ obtained with the numerical fluxes (5.9) (REL), (5.5) (HLL), (5.3) (GOD), and the Roe solver for a monocomponent perfect gas (ROE-PG), on two grids with $N = 100$ and $N = 800$ elements.

a 5 species model with a uniform composition $Y_{N_2} = 0.7543$, $Y_{O_2} = 0.2283$, $Y_{NO} = 0.01026$, $Y_N = 6.5 \times 10^{-7}$, and $Y_O = 0.00713$. We neglect the enthalpies of formation so the gas is a perfect gas with an equivalent adiabatic exponent $\gamma(\mathbf{Y}) = 1.402$ and we compare our results to the Roe solver for a perfect gas with an adiabatic exponent of 1.402 (ROE-PG). Results in fig. 6.2 show that all solvers provide similar results and converge to the entropy weak solution. We stress that in spite of the crude assumption $\gamma > \frac{5}{3}$ in the numerical fluxes from section 5 they offer similar accuracy as the Roe solver.

6.2 Hypersonic flow over a sphere

We now consider the 2D hypersonic flow over a $\frac{1}{4}$ inch diameter sphere with the freestream conditions of Lobb's experiments [35]. The freestream Mach number is $M_\infty = \frac{u_\infty}{c_\infty} = 15.3$ with $\rho_\infty = 7.83 \times 10^{-3} \text{ kg/m}^3$ and $T_\infty = 293\text{K}$. The upstream flow is made of nitrogen and oxygen with $Y_{N_2} = 0.79$, $Y_{O_2} = 0.21$ which are uniform in the flow domain since we do not consider chemical reactions or molecular relaxation. The freestream vibration temperatures are taken at T_∞ for both species. A symmetry condition is imposed at the bottom boundary.

Figure 6.4 displays the contours of Mach number and translation-rotation temperature on two different grids with the three different schemes. Neglecting chemical reactions overestimates the shock distance to the sphere and prevents comparison to Lobb's experiments. As we do not consider chemical reactions or

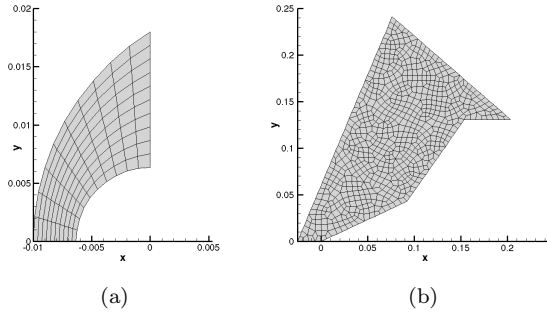


Fig. 6.3: Examples of meshes for the 2D simulations: hypersonic flows over (a) a sphere with $N = 100$ elements, (b) a double cone with $N = 749$ elements.

molecular relaxation, a partial validation of the current results can be obtained by comparison with simulations of an equivalent monocomponent perfect gas with adiabatic exponent $\gamma = 1.4$. The simulations of the considered gas mixture using the numerical flux (5.5) and of the equivalent perfect gas using the HLL flux for polytropic gas dynamics (HLL-PG) are reported in fig. 6.5. As expected, while some differences can be identified for underresolved simulations, the results are almost perfectly overlapping for sufficiently fine resolutions.

We are however interested in comparing results obtained with the different schemes and analysing their convergence under grid refinement. To this end we compare the convergence of shock distance from the sphere in fig. 6.6. We use grids with $N = 20 \times 20$, 40×40 , 80×80 and 160×160 elements for the simulation (see fig. 6.3), while the reference distance x_{ref} is evaluated with the Godunov numerical flux on a fine mesh with $N = 320 \times 320$. The results confirm convergence of the shock position and highlight close values obtained with the three different schemes.

6.3 Hypersonic flow over a double cone

We finally consider the 2D hypersonic flow over a double cone with angles 25 and 55 deg. adapted from [15, 32] and made of molecular and atomic nitrogen with mass fractions $Y_{N_2} = 0.99$, $Y_N = 0.01$. The freestream Mach number is $M_\infty = 11.3$ with $\rho_\infty = 1.34 \times 10^{-3} \text{kg/m}^3$ and $T_\infty = 303\text{K}$. The freestream vibration temperature of the molecular nitrogen is taken at $T_{N_2_\infty} = 3085\text{K}$. We use a series of five unstructured grids (see fig. 6.3). A symmetry condition is imposed at the bottom boundary.

Contours of Mach number and translation-rotation temperature obtained with the three different schemes on the second finest mesh are displayed in fig. 6.7. Compared to references [15, 32], we observe a strong overestimation of the distance of the bow shock to the wall due to the absence of chemical reactions. However, the results with the three schemes are in good agreement. As done for the previous configuration, we compare in fig. 6.8 the obtained solution to that corresponding to the use of an equivalent perfect gas with adiabatic exponent $\gamma = 1.4032$ (HLL-PG)

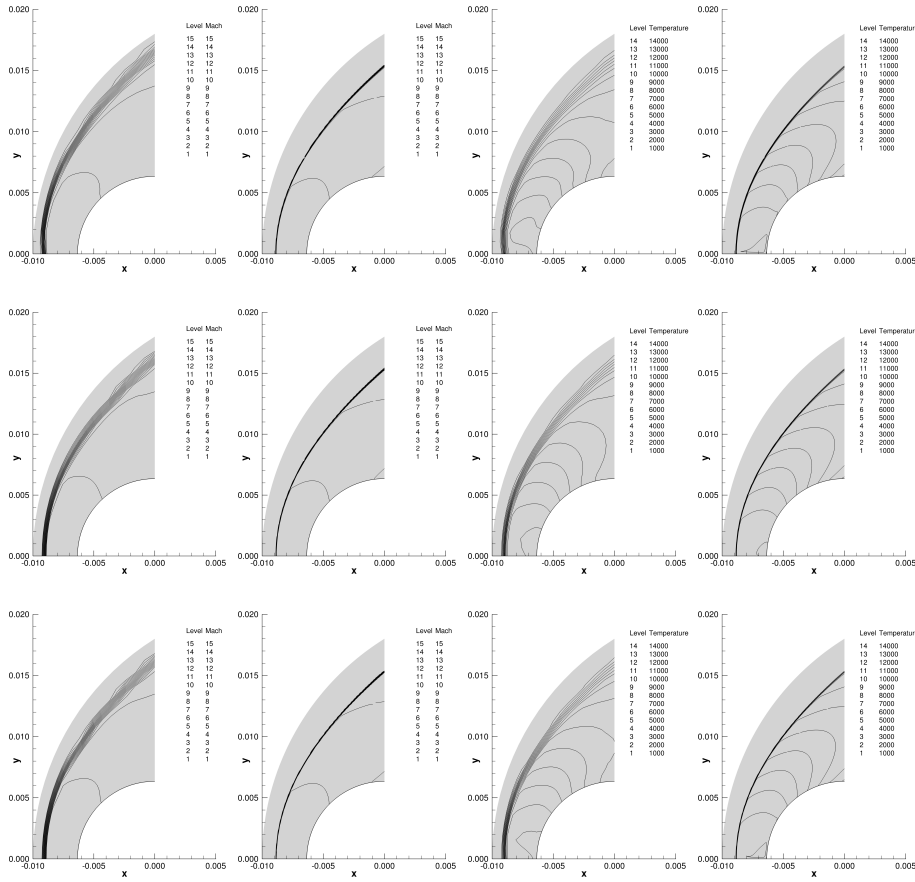


Fig. 6.4: Hypersonic flow over Lobb's sphere: Mach number M and temperature T contours obtained with the numerical fluxes (5.9) (top row), (5.5) (middle row), (5.3) (bottom row), on two grids with $N = 20 \times 20$ and 160×160 elements.

on a fine grid. Once again a very good agreement is obtained. Finally in fig. 6.9, we display the pressure distribution at the wall obtained with the schemes on the five grids. The first pressure peak corresponds to the reflexion of the separated shock at the wall, while the second peak corresponds to rapid pressure variations due to the geometrical transition between the cones. We observe convergence of the solution as the mesh is refined and a close agreement between results from the three schemes on the finest grids.

7 Concluding remarks

We introduce a general framework to design finite volume schemes for the compressible multicomponent Euler equations in thermal nonequilibrium. The frame-

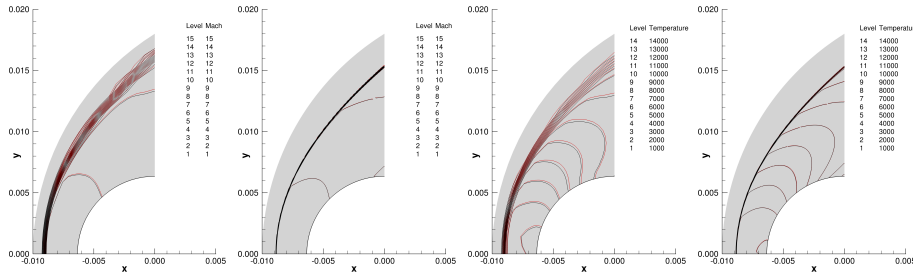


Fig. 6.5: Hypersonic flow over Lobb’s sphere: Mach number M and temperature T contours obtained with the HLL numerical flux (5.5) (red), and the HLL-PG flux considering an equivalent monocomponent perfect gas (black) on two grids with $N = 20 \times 20$ and 160×160 elements.

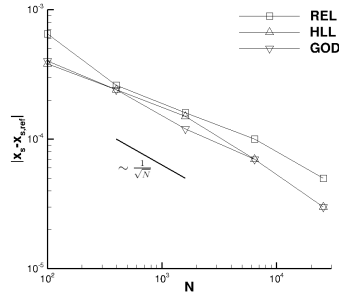


Fig. 6.6: Hypersonic flow over Lobb’s sphere: convergence of the shock position in the symmetry plane $y = 0$ under mesh refinement.

work allows to define a numerical scheme for its discretization from a scheme for the discretization of the monocomponent polytropic gas dynamics through a simple linear formula. Moreover, the numerical scheme inherits the properties of the scheme for the polytropic gas dynamics under a subcharacteristic condition on the adiabatic exponent of the polytropic gas.

This framework relies on the extension of the relaxation of energy for the gas dynamics equations [11] to the model under consideration in this work. Three different numerical fluxes are constructed with this framework the polytropic Godunov exact Riemann solver [23], HLL numerical flux [27], and pressure-based relaxation solver [3]. They are assessed through numerical simulations of flows in one and two space dimensions with discontinuous solutions and complex wave interactions. The results highlight robustness, nonlinear stability, convergence of the present method, as well as similar performances of the three schemes.

Other numerical fluxes may be deduced from this framework. We also stress that the numerical fluxes designed in this framework can be used as building blocks in the general framework of conservative elementwise flux differencing schemes

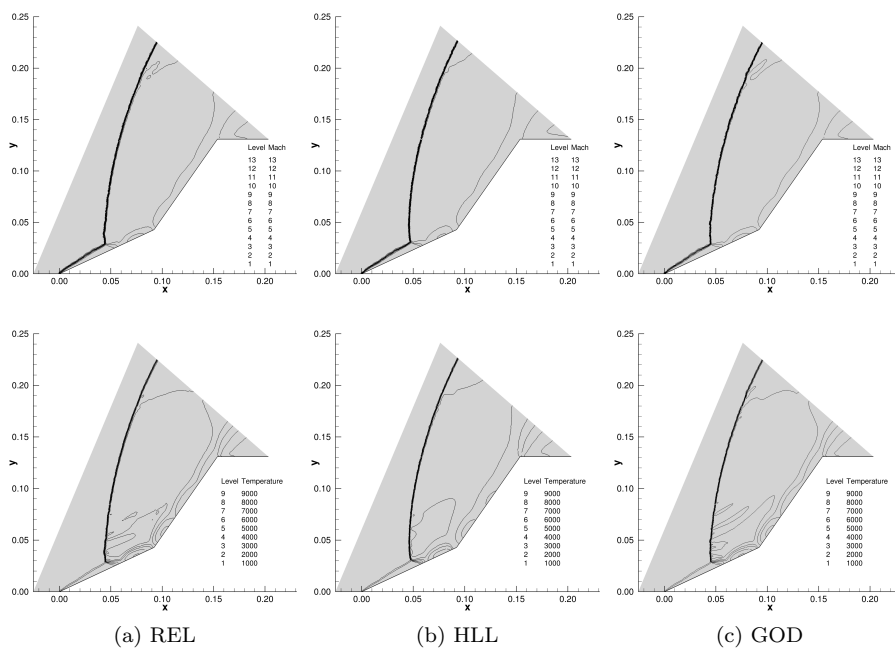


Fig. 6.7: Hypersonic flow over a double cone: Mach number M (top row) and temperature T (bottom row) contours obtained with the numerical fluxes (5.9) (REL), (5.5) (HLL), and (5.3) (GOD) on a fine grid with $N = 52,237$ elements.

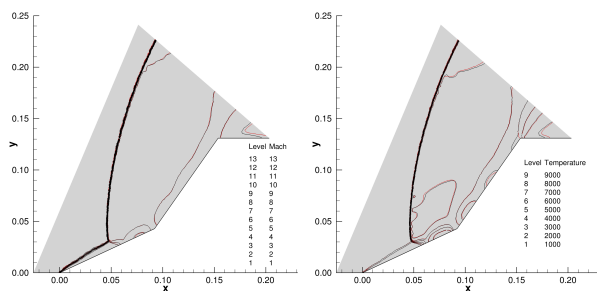


Fig. 6.8: Hypersonic flow over a double cone: Mach number M (left) and temperature T (right) contours obtained with the numerical flux (5.5) (red), and the HLL-PG flux considering an equivalent perfect gas (black) on a fine grid with $N = 52,237$ elements.

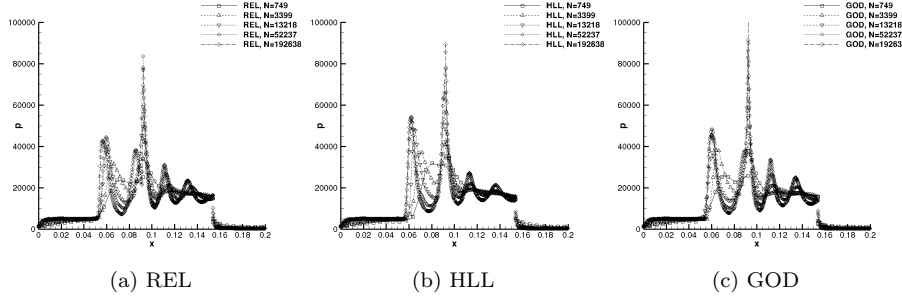


Fig. 6.9: Hypersonic flow over a double cone: pressure distribution at the wall obtained with the numerical fluxes (5.9) (REL), (5.5) (HLL), and (5.3) (GOD) on a series of five grids with N elements.

[17] and future work will consider the use of discontinuous Galerkin schemes for the discretization of the compressible multicomponent Euler equations in thermal nonequilibrium.

A Convexity of the entropy for the energy relaxation system

The object of this appendix is the proof of lemma 4.2. Without loss of generality we define n_s in the mapping (4.12) as the one corresponding to one species that satisfies $r_{n_s} = \min_{\alpha} r_{\alpha}$. To prove that $\rho\zeta(\mathbf{w})$ is convex it is sufficient to prove that $\zeta(\mathcal{Y}, \tau, e_r, e_s, \mathbf{e}_v)$ is convex from lemma 4.1 and, from (4.14), we rewrite ζ as

$$\begin{aligned} \zeta(\mathcal{Y}, \tau, e_r, e_s, \mathbf{e}_v) &= C_{v_t}(\mathcal{Y}) \ln((\gamma - \gamma(\mathcal{Y}))C_{v_t}(\mathcal{Y})) + \sum_{\alpha=1}^{n_s} r_{\alpha} Y_{\alpha} \ln Y_{\alpha} + \frac{r(\mathcal{Y})}{\gamma-1} \ln \frac{\gamma(\mathcal{Y})-1}{\gamma-\gamma(\mathcal{Y})} \\ &\quad - r(\mathcal{Y}) \ln \tau - \frac{r(\mathcal{Y})}{\gamma-1} \ln e_r - \frac{(\gamma-\gamma(\mathcal{Y}))C_{v_t}(\mathcal{Y})}{\gamma-1} \ln e_s + l(\mathcal{Y}) - s_v(\mathbf{Y}, \mathbf{e}_v), \end{aligned}$$

with $l(\mathcal{Y}) = -\sum_{\alpha} Y_{\alpha} C_{v_{\alpha}}^t \ln C_{v_{\alpha}}^t - C_{v_t}(\mathcal{Y}) \ln(\gamma - 1)$, with $Y_{n_s} = 1 - \sum_{\alpha < n_s} Y_{\alpha}$, linear in \mathcal{Y} .

Introducing the short notations $\partial_k r \equiv \partial_{Y_k} r(\mathcal{Y})$, $\partial_k C_{v_t} \equiv \partial_{Y_k} C_{v_t}(\mathcal{Y})$, and $\partial_k \gamma \equiv \partial_{Y_k} \gamma(\mathcal{Y})$, the Hessian $\mathcal{H}_{\zeta}(\mathcal{Y}, \tau, e_r, e_s, \mathbf{e}_v)$ of ζ reads

$$\begin{pmatrix} (\partial_{kl}^2 \zeta - \delta_{k,l} \psi_k \frac{e_k^v s_k''(e_k^v)}{Y_k})_{kl} & (\frac{-\partial_k r}{\tau})_k & (\frac{-\partial_k r}{(\gamma-1)e_r})_k & (\frac{\partial_k r - (\gamma-1)\partial_k C_{v_t}}{(\gamma-1)e_s})_k & (\frac{e_k^v s_k''(e_k^v)}{Y_k})_{1 \leq k \leq n_d} \\ (\frac{-\partial_l r}{\tau})_l & \frac{r(\mathcal{Y})}{\tau^2} & 0 & 0 & 0 \\ (\frac{-\partial_l r}{(\gamma-1)e_r})_l & 0 & \frac{r(\mathcal{Y})}{(\gamma-1)e_r^2} & 0 & 0 \\ (\frac{\partial_l r - (\gamma-1)\partial_l C_{v_t}}{(\gamma-1)e_s})_l & 0 & 0 & \frac{\gamma-\gamma(\mathcal{Y})}{\gamma-1} \frac{C_{v_t}(\mathcal{Y})}{e_s^2} & 0 \\ (\frac{e_l^v s_l''(e_l^v)}{Y_l})_{1 \leq l \leq n_d} & 0 & 0 & 0 & (-\delta_{k,l} \frac{s_k''(e_k^v)}{Y_k})_{k,l} \end{pmatrix} \quad (\text{A.1})$$

with $\delta_{k,l}$ the Kronecker symbol and $\psi_k = 1$ if $1 \leq k \leq n_d$ and $\psi_k = 0$ if $n_d < k \leq n_s$. Unless stated otherwise, the subscripts are in the range $1 \leq k, l < n_s$, k corresponding to a row index and l corresponding to a column index. Likewise

$$\partial_k r \stackrel{(2.9)}{=} C_{v_t}(\mathcal{Y}) \partial_k \gamma + (\gamma(\mathcal{Y}) - 1) \partial_k C_{v_t}, \quad (\text{A.2})$$

and

$$\partial_{kl}^2 \zeta = \frac{r_{n_s}}{Y_{n_s}} + \frac{r_k}{Y_k} \delta_{k,l} + \frac{\partial_k C_{v_t} \partial_l C_{v_t}}{C_{v_t}(\mathbf{Y})} + \frac{C_{v_t}(\mathbf{Y}) \partial_k \gamma \partial_l \gamma}{(\gamma - \gamma(\mathbf{Y}))(\gamma(\mathbf{Y}) - 1)}, \quad 1 \leq k, l < n_s. \quad (\text{A.3})$$

We now prove that \mathcal{H}_ζ is symmetric positive definite. Let $\mathbf{x} = (x_{1 \leq i < n_s}, x_\tau, x_r, x_s, x_{1 \leq i \leq n_d}^v)^\top$ in $\mathbb{R}^{n_s + n_d + 3}$ non zero and use the notation $\sum \equiv \sum_{k=1}^{n_s-1}$, we get

$$\begin{aligned} \sum_{k,l=1}^{n_s-1} x_k \partial_{kl}^2 \zeta x_l &\stackrel{(\text{A.3})}{=} \frac{r_{n_s} (\sum x_k)^2}{Y_{n_s}} + \sum \frac{r_k x_k^2}{Y_k} + \frac{(\sum x_k \partial_k C_{v_t})^2}{C_{v_t}(\mathbf{Y})} + \frac{C_{v_t}(\mathbf{Y}) (\sum x_k \partial_k \gamma)^2}{(\gamma - \gamma(\mathbf{Y}))(\gamma(\mathbf{Y}) - 1)} \\ &\stackrel{(\text{A.2})}{=} \frac{r_{n_s} (\sum x_k)^2}{Y_{n_s}} + \sum \frac{r_k x_k^2}{Y_k} + \frac{(\sum x_k \partial_k C_{v_t})^2}{C_{v_t}(\mathbf{Y})} \\ &\quad + \frac{\left(\sum x_k (\partial_k r - (\gamma(\mathbf{Y}) - 1) \partial_k C_{v_t}) \right)^2}{(\gamma - \gamma(\mathbf{Y})) r(\mathbf{Y})} \\ &= \frac{r_{n_s} (\sum x_k)^2}{Y_{n_s}} + \sum \frac{r_k x_k^2}{Y_k} + \frac{(\sum x_k \partial_k C_{v_t})^2}{C_{v_t}(\mathbf{Y})} \\ &\quad + \frac{(\sum x_k \partial_k r)^2}{(\gamma - \gamma(\mathbf{Y})) r(\mathbf{Y})} + \frac{(\gamma(\mathbf{Y}) - 1) (\sum x_k \partial_k C_{v_t})^2}{(\gamma - \gamma(\mathbf{Y})) C_{v_t}(\mathbf{Y})} - \frac{2(\sum x_k \partial_k r) (\sum x_k \partial_k C_{v_t})}{(\gamma - \gamma(\mathbf{Y})) C_{v_t}(\mathbf{Y})} \\ &\stackrel{(\text{A.2})}{=} \frac{r_{n_s} (\sum x_k)^2}{Y_{n_s}} + \sum \frac{r_k x_k^2}{Y_k} + \frac{(\sum x_k \partial_k r)^2}{(\gamma - 1) r(\mathbf{Y})} + \frac{(\sum x_k (\gamma - 1) \partial_k C_{v_t} - x_k \partial_k r)^2}{(\gamma - \gamma(\mathbf{Y})) (\gamma - 1) C_{v_t}(\mathbf{Y})}, \end{aligned} \quad (\text{A.4})$$

so using (A.1) and (A.4) we obtain

$$\begin{aligned} \mathbf{x}^\top \mathcal{H}_\zeta \mathbf{x} &= \frac{r_{n_s} (\sum x_k)^2}{Y_{n_s}} + \sum \frac{r_k x_k^2}{Y_k} + \left(1 + \frac{1}{\gamma - 1} - 1\right) \frac{(\sum x_k \partial_k r)^2}{r(\mathbf{Y})} - \sum_{k=1}^{n_d} \frac{s_k^{v''}(e_k^v)}{Y_k} (x_k^v - e_k^v x_k)^2 \\ &\quad + \frac{(\sum x_k (\gamma - 1) \partial_k C_{v_t} - x_k \partial_k r)^2}{(\gamma - \gamma(\mathbf{Y})) (\gamma - 1) C_{v_t}(\mathbf{Y})} + r(\mathbf{Y}) \frac{x_\tau^2}{\tau^2} + \frac{r(\mathbf{Y})}{\gamma - 1} \frac{x_r^2}{e_r^2} \\ &\quad + \frac{(\gamma - \gamma(\mathbf{Y})) C_{v_t}(\mathbf{Y})}{\gamma - 1} \frac{x_s^2}{e_s^2} - 2 \sum x_k \left(\partial_k r \frac{x_\tau}{\tau} + \frac{\partial_k r}{\gamma - 1} \frac{x_r}{e_r} + \frac{(\gamma - 1) \partial_k C_{v_t} - \partial_k r}{\gamma - 1} \frac{x_s}{e_s} \right) \\ &= Q(\mathbf{x}) + \frac{(\sum x_k \partial_k r - r(\mathbf{Y}) \frac{x_\tau}{\tau})^2}{r(\mathbf{Y})} + \frac{(\sum x_k \partial_k r - r(\mathbf{Y}) \frac{x_r}{e_r})^2}{(\gamma - 1) r(\mathbf{Y})} \\ &\quad + \frac{(\sum x_k ((\gamma - 1) \partial_k C_{v_t} - \partial_k r) - (\gamma - \gamma(\mathbf{Y})) C_{v_t}(\mathbf{Y}) \frac{x_s}{e_s})^2}{(\gamma - \gamma(\mathbf{Y})) (\gamma - 1) C_{v_t}(\mathbf{Y})} - \sum_{k=1}^{n_d} \frac{s_k^{v''}(e_k^v)}{Y_k} (x_k^v - e_k^v x_k)^2, \end{aligned}$$

with $s_k^{v''}(e_k^v) = -\frac{r_k}{e_k^v (e_k^v + r_k \partial_k^v)} < 0$, so the four last terms are non-negative, and

$$Q(\mathbf{x}) = \frac{r_{n_s} (\sum x_k)^2}{Y_{n_s}} + \sum \frac{r_k x_k^2}{Y_k} - \frac{(\sum x_k \partial_k r)^2}{r(\mathbf{Y})}.$$

Using (4.13), we get $\partial_k r = r_k - r_{n_s} \geq 0$ since by assumption $r_{n_s} = \min_\alpha r_\alpha$, so we rewrite

$$\sum \frac{r_k x_k^2}{Y_k} = \sum \frac{r_{n_s} + \partial_k r}{Y_k} x_k^2 = \sum \frac{r_{n_s}}{Y_k} x_k^2 + \sum \frac{r_{n_s} + \sum_l Y_l \partial_l r}{r(\mathbf{Y})} \frac{\partial_k r}{Y_k} x_k^2,$$

and hence obtain

$$\begin{aligned} Q(\mathbf{x}) &= \frac{r_{n_s} (\sum x_k)^2}{Y_{n_s}} + \sum \frac{r_{n_s}}{Y_k} \left(1 + \frac{\partial_k r}{r(\mathbf{Y})}\right) x_k^2 + \sum_{k,l=1}^{n_s-1} \frac{\partial_k r \partial_l r}{r(\mathbf{Y})} \left(\frac{Y_l}{Y_k} x_k^2 - x_k x_l\right) \\ &= \frac{r_{n_s} (\sum x_k)^2}{Y_{n_s}} + \sum \frac{r_{n_s}}{Y_k} \left(1 + \frac{\partial_k r}{r(\mathbf{Y})}\right) x_k^2 + \frac{1}{2} \sum_{k,l=1}^{n_s-1} \frac{\partial_k r \partial_l r Y_k Y_l}{r(\mathbf{Y})} \left(\frac{x_k}{Y_k} - \frac{x_l}{Y_l}\right)^2, \end{aligned}$$

which is positive, providing that the $x_{1 \leq k < n_s}$ are not all zero since $\partial_k r \geq 0$, so $\mathbf{x}^\top \mathcal{H}_\zeta \mathbf{x} > 0$ and we conclude that $\zeta(\mathcal{Y}, \tau, e_r, e_s, e_v)$ is strictly convex. \square

Acknowledgements Part of this work was funded under the Onera research project JER-OBOAM. One of the authors (F. Renac) gratefully acknowledges this support.

References

1. Abgrall, R.: How to prevent pressure oscillations in multicomponent flow calculations: a quasi conservative approach. *J. Comput. Phys.* **125**(1), 150–160 (1996)
2. Anderson Jr., J.D.: *Hypersonic and High Temperature Gas Dynamics*. McGraw-Hill Book Company, New-York (1989)
3. Bouchut, F.: *Nonlinear Stability of Finite Volume Methods for Hyperbolic Conservation Laws and Well-Balanced Schemes for Sources*. *Frontiers in Mathematics*. Birkhäuser Basel (2004)
4. Candler, G.V., MacCormack, R.W.: Computation of weakly ionized hypersonic flows in thermochemical nonequilibrium. *J. Thermophys. Heat. Trans.* **5**(3), 266–273 (1991). DOI 10.2514/3.260
5. Chen, G.Q., Levermore, C.D., Liu, T.P.: Hyperbolic conservation laws with stiff relaxation terms and entropy. *Comm. Pure Appl. Math.* **47**(6), 787–830 (1994)
6. Ciarlet, P.: *The Finite Element Method for Elliptic Problems*. *Classics in Applied Mathematics*. Society for Industrial and Applied Mathematics (2002). URL <https://books.google.fr/books?id=isEEyUXW9qkC>
7. Colella, P., Glaz, H.M.: Efficient solution algorithms for the Riemann problem for real gases. *J. Comput. Phys.* **59**(2), 264–289 (1985). DOI [https://doi.org/10.1016/0021-9991\(85\)90146-9](https://doi.org/10.1016/0021-9991(85)90146-9)
8. Coquel, F., Godlewski, E., Perthame, B., In, A., Rascle, P.: *Some New Godunov and Relaxation Methods for Two-Phase Flow Problems*, pp. 179–188. Springer US, Boston, MA (2001)
9. Coquel, F., Godlewski, E., Seguin, N.: Relaxation of fluid systems. *Math. Models Methods Appl. Science* **22**(08), 1250,014 (2012). DOI 10.1142/S0218202512500145
10. Coquel, F., Marmignon, C.: A Roe-type linearization for the Euler equations for weakly ionized multi-component and multi-temperature gas (1995). DOI 10.2514/6.1995-1675
11. Coquel, F., Perthame, B.: Relaxation of energy and approximate Riemann solvers for general pressure laws in fluid dynamics. *SIAM J. Numer. Anal.* **35**(6), 2223–2249 (1998)
12. Dafermos, C.M.: *Hyperbolic Conservation Laws in Continuum Physics*. *Grundlehren der mathematischen Wissenschaften*. Springer Berlin Heidelberg, Berlin, Heidelberg (2016)
13. Dellacherie, Stéphane: Relaxation schemes for the multicomponent Euler system. *ESAIM: M2AN* **37**(6), 909–936 (2003). DOI 10.1051/m2an:2003061. URL <https://doi.org/10.1051/m2an:2003061>
14. Drikakis, D.: Advances in turbulent flow computations using high-resolution methods. *Progress in Aerospace Sciences* **39**(6), 405–424 (2003). DOI [https://doi.org/10.1016/S0376-0421\(03\)00075-7](https://doi.org/10.1016/S0376-0421(03)00075-7)
15. Druguet, M.C., Candler, G.V., Nompelis, I.: Effects of numerics on Navier-Stokes computations of hypersonic double-cone flows. *AIAA Journal* **43**(3), 616–623 (2005). DOI 10.2514/1.6190
16. Einfeldt, B., Munz, C., Roe, P., Sjögren, B.: On Godunov-type methods near low densities. *J. Comput. Phys.* **92**(2), 273 – 295 (1991)
17. Fisher, T.C., Carpenter, M.H.: High-order entropy stable finite difference schemes for nonlinear conservation laws: Finite domains. *J. Comput. Phys.* **252**, 518–557 (2013)
18. Flament, C., Prud’homme, R.: Entropy and entropy production in thermal and chemical non-equilibrium flows. *J. Non-Equilib. Thermodyn.* **18**(4), 295–310 (1993). DOI <https://doi.org/10.1515/jnet.1993.18.4.295>. URL <https://www.degruyter.com/view/journals/jnet/18/4/article-p295.xml>
19. Gaitonde, D.: *An Assessment of CFD for Prediction of 2-D and 3-D High-Speed Flows* (2012). DOI 10.2514/6.2010-1284
20. Giovangigli, V.: *Multicomponent Flow Modeling*. *Modeling and Simulation in Science, Engineering and Technology*. Birkhäuser Basel (1999)

21. Glaister, P.: An approximate linearised Riemann solver for the three-dimensional Euler equations for real gases using operator splitting. *J. Comput. Phys.* **77**(2), 361–383 (1988). DOI [https://doi.org/10.1016/0021-9991\(88\)90174-X](https://doi.org/10.1016/0021-9991(88)90174-X)
22. Godlewski, E., Raviart, P.A.: Numerical approximation of hyperbolic systems of conservation laws. *Applied Mathematical Sciences*, vol. 118. Springer-Verlag, New-York (1996)
23. Godunov, S.: A difference scheme for numerical computation of discontinuous solutions of equations of fluid dynamics. *Math. USSR Sbornik* **47**, 271–306 (1959)
24. Gouasmi, Ayoub, Duraisamy, Karthik, Murman, Scott M., Tadmor, Eitan: A minimum entropy principle in the compressible multicomponent Euler equations. *ESAIM: M2AN* **54**(2), 373–389 (2020). DOI 10.1051/m2an/2019070. URL <https://doi.org/10.1051/m2an/2019070>
25. Guermond, J.L., Popov, B.: Fast estimation from above of the maximum wave speed in the Riemann problem for the Euler equations. *J. Comput. Phys.* **321**, 908–926 (2016). DOI <https://doi.org/10.1016/j.jcp.2016.05.054>. URL <http://www.sciencedirect.com/science/article/pii/S0021999116301991>
26. Harten, A., Hyman, J.M.: Self adjusting grid methods for one-dimensional hyperbolic conservation laws. *J. Comput. Phys.* **50**(2), 235–269 (1983). DOI [https://doi.org/10.1016/0021-9991\(83\)90066-9](https://doi.org/10.1016/0021-9991(83)90066-9)
27. Harten, A., Lax, P.D., van Leer, B.: On upstream differencing and Godunov-type schemes for hyperbolic conservation laws. *SIAM Rev.* **25**(1), 35–61 (1983)
28. Harten, A., Lax, P.D., Levermore, C.D., Morokoff, W.J.: Convex entropies and hyperbolicity for general Euler equations. *SIAM J. Numer. Anal.* **35**(6), 2117–2127 (1998). DOI 10.1137/S0036142997316700
29. Henneton, M., Gainville, O., Coulouvrat, F.: Numerical simulation of sonic boom from hypersonic meteoroids. *AIAA Journal* **53**(9), 2560–2570 (2015)
30. Honma, H., Glass, I.L.: Weak spherical shock-wave transitions of n-waves in air with vibrational excitation. *Proceedings of the Royal Society of London. Series A, Mathematical and Physical Sciences* **391**(1800), 55–83 (1984)
31. Karni, S.: Hybrid multifluid algorithms. *SIAM J. Sci. Comput.* **17**(5), 1019–1039 (1996). DOI 10.1137/S106482759528003X
32. Knight, D., Longo, J., Drikakis, D., Gaitonde, D., Lani, A., Nompelis, I., Reimann, B., Walpot, L.: Assessment of cfd capability for prediction of hypersonic shock interactions. *Progress in Aerospace Sciences* **48-49**, 8–26 (2012). Assessment of Aerothermodynamic Flight Prediction Tools
33. Knisely, C.P., Zhong, X.: Sound radiation by supersonic unstable modes in hypersonic blunt cone boundary layers. ii. direct numerical simulation. *Physics of Fluids* **31**(2), 024,104 (2019)
34. Liu, Y., Vinokur, M.: Nonequilibrium flow computations. i. an analysis of numerical formulations of conservation laws. *J. Comput. Phys.* **83**(2), 373–397 (1989). DOI [https://doi.org/10.1016/0021-9991\(89\)90125-3](https://doi.org/10.1016/0021-9991(89)90125-3). URL <http://www.sciencedirect.com/science/article/pii/0021999189901253>
35. LOBB, R.K.: Chapter 26 - experimental measurement of shock detachment distance on spheres fired in air at hypervelocities. In: W.C. NELSON (ed.) *The High Temperature Aspects of Hypersonic Flow, AGARDograph*, vol. 68, pp. 519–527. Elsevier (1964). DOI <https://doi.org/10.1016/B978-1-4831-9828-6.50031-X>
36. PARK, C.: On convergence of computation of chemically reacting flows (1985). DOI 10.2514/6.1985-247
37. Park, C.: *Nonequilibrium Hypersonic Aerothermodynamics*. Springer-Verlag, New-York (1990)
38. Perthame, B., Shu, C.W.: On positivity preserving finite volume schemes for Euler equations. *Numer. Math.* **73**(1), 119–130 (1996)
39. Prakash, A., Parsons, N., Wang, X., Zhong, X.: High-order shock-fitting methods for direct numerical simulation of hypersonic flow with chemical and thermal nonequilibrium. *J. Comput. Phys.* **230**(23), 8474–8507 (2011)
40. Renac, F.: Entropy stable, robust and high-order DGSEM for the compressible multicomponent Euler equations. submitted (2020)
41. Renac, F., de la Llave Plata, M., Martin, E., Chapelier, J.B., Couaillier, V.: Aghora: A High-Order DG Solver for Turbulent Flow Simulations, pp. 315–335. Springer International Publishing, Cham (2015)
42. Roe, P.: Approximate Riemann solvers, parameter vectors, and difference schemes. *J. Comput. Phys.* **43**(2), 357–372 (1981). DOI [https://doi.org/10.1016/0021-9991\(81\)90128-5](https://doi.org/10.1016/0021-9991(81)90128-5)

43. Rouzaud, O., Chalons, C., Marmignon, C., Soubri'e, T.: Development of a Relaxation Scheme for Weakly Ionised Gases (2005). DOI <https://doi.org/10.2514/6.2005-603>
44. Rusanov, V.: Calculation of interaction of non-steady shock waves with obstacles. *J. Comp. Math. Phys. USSR* **1**, 267–279 (1961)
45. Shuen, J.S., Liou, M.S., Leer, B.V.: Inviscid flux-splitting algorithms for real gases with non-equilibrium chemistry. *J. Comput. Phys.* **90**(2), 371–395 (1990). DOI [https://doi.org/10.1016/0021-9991\(90\)90172-W](https://doi.org/10.1016/0021-9991(90)90172-W)
46. Svärd, M., Özcan, H.: Entropy-stable schemes for the Euler equations with far-field and wall boundary conditions. *J. Sci. Comput.* **58**, 61–89 (2014)
47. Tadmor, E.: A minimum entropy principle in the gas dynamics equations. *Appl. Numer. Math.* **6**, 211–219 (1986)
48. Tadmor, E.: The numerical viscosity of entropy stable schemes for systems of conservation laws. i. *Math. Comput.* **49**(179), 91–103 (1987)
49. Tadmor, E.: Entropy stability theory for difference approximations of nonlinear conservation laws and related time-dependent problems. *Acta Numerica* **12**, 451–512 (2003)
50. Ton, V.T.: Improved shock-capturing methods for multicomponent and reacting flows. *J. Comput. Phys.* **128**(1), 237–253 (1996). DOI <https://doi.org/10.1006/jcph.1996.0206>
51. Toro, E.F.: *Riemann Solvers and Numerical Methods for Fluid Dynamics: A Practical Introduction*. Third Edition. Springer-Verlag Berlin Heidelberg (2009)